Conserved cell-type specific signature of resilience to Alzheimer's disease nominates role for excitatory cortical neurons

Maria A. Telpoukhovskaia[1], Niran Hadad[1], Brianna Gurdon[1,2], Miko Dai[1], Andrew R. Ouellette[1,2], Sarah M. Neuner[3], Amy R. Dunn[1], Shania Hansen[4,5], Yiyang Wu[4,5], Logan Dumitrescu[4,5], Kristen M.S. O'Connell[1,2,6], Eric B. Dammer[7], Nicholas T. Seyfried[7,8], Sukalp Muzumdar[9], Jesse Gillis[9,10], Paul Robson[11,12,13], Ji-Gang Zhang[1], Timothy J. Hohman[4,5], Vivek M. Philip[1], Vilas Menon[14*], Catherine C. Kaczorowski[1,2,6*]

1. The Jackson Laboratory for Mammalian Genetics, Bar Harbor, ME, USA;
2. Graduate School of Biomedical Science and Engineering, University of Maine, Orono, ME, USA;
3. Department of Genetics and Genomic Sciences, Icahn School of Medicine at Mount Sinai, New York, NY;
4. Vanderbilt Memory and Alzheimer's Center, Vanderbilt University Medical Center, Nashville, TN, USA;
5. Department of Neurology, Vanderbilt University Medical Center, Nashville, TN, USA;
6. Neuroscience Program, Graduate School of Biomedical Science, Tufts University School of Medicine, Boston, MA, USA;
7. Department of Biochemistry, Emory University School of Medicine, Atlanta, GA, USA;
8. Department of Neurology, Emory University School of Medicine, Atlanta, GA, USA;
9. Cold Spring Harbor Laboratory, Cold Spring Harbor, NY, USA;
10. Department of Physiology, University of Toronto, Toronto, Ontario, Canada;
11. The Jackson Laboratory for Genomic Medicine, Farmington, CT, USA;
12. Department of Genetics and Genome Sciences, University of Connecticut Health Center, Farmington, CT, USA;
13. Institute for Systems Genomics, University of Connecticut, Farmington, CT, USA;
14. Department of Neurology, Center for Translational and Computational Neuroimmunology, Columbia University Irving Medical Center, New York City, NY, USA.

*Co-senior and corresponding authors. Email: catherine.kaczorowski@jax.org (C.C.K.); vm2545@cumc.columbia.edu (V.M.)

Abstract

Alzheimer's disease (AD), the leading cause of dementia, affects millions of people worldwide. With no disease-modifying medication currently available, the human toll and economic costs are rising rapidly. Under current standards, a patient is diagnosed with AD when both cognitive decline and pathology (amyloid plaques and neurofibrillary tangles) are present. Remarkably, some individuals who have AD pathology remain cognitively normal. Uncovering factors that lead to "cognitive resilience" to AD is a promising path to create new targets for therapies. However, technical challenges discovering novel human resilience factors limit testing, validation, and nomination of novel drugs for AD. In this study, we use single-nuclear transcriptional profiles of postmortem cortex from human individuals with high AD pathology who were either cognitively normal (resilient) or cognitively impaired (susceptible) at time of death, as well as mouse strains that parallel these differences in cognition with high amyloid. Our cross-species discovery approach highlights a novel role for excitatory layer 4/5 cortical neurons in promoting cognitive resilience to AD, and nominates several resilience genes that include *ATP1A1*, *GABRB1*, *PTK2*, and *ROCK2*. Nominated resilience genes were tested for replication in orthogonal data sets and confirmed to be correlated with cognitive resilience. Additionally, we identified several potential mechanisms of resilience, including regulation of membrane potential, axonal and dendritic growth, and general increase of protein cycle, potentially of membrane proteins. Because our discovery of resilience-associated genes in layer 4/5 cortical neurons originates from an integrated human and mouse transcriptomic space from susceptible and resilient individuals, we are positioned to test causality and perform mechanistic, validation, and pre-clinical studies in our human-relevant AD-BXD mouse panel.

Introduction

Resilience to cognitive decline associated with Alzheimer's disease (AD) is a phenomenon by which some people retain better than expected cognitive ability despite high amyloid and tau burdens (Arenaza-Urquijo and Vemuri, 2018). Bolstering the brain's ability to cope with AD pathology is an attractive new avenue for therapies. Resilience to AD has been reported in longitudinal cohort studies, such as in the Religious Orders Study (ROS) and Memory and Aging Project (MAP) groups, in which a third of individuals with normal cognition have AD pathology (Bennett et al., 2012a; Bennett et al., 2012b). While some resilience factors have been identified by studying these individuals (Arnold et al., 2013; Negash et al., 2013; Yu et al., 2020), many resilience factors and the mechanisms by which they act remain unknown or poorly understood, particularly in the context of specific cell types and their contribution to resilience. In parallel, translationally relevant model organisms are essential to validate and test resilience candidates, and genetically diverse mouse models are valuable for modeling complex diseases (Neuner et al., 2022; Saul et al., 2019).

The AD-BXDs are a panel of mice that incorporates the 5XFAD mutation into the genetically diverse BXD genetic reference panel. This panel models individual differences in memory function in response to human FAD mutations, resulting in a genetically diverse population of AD mice that is sensitive to additive effects of inherited risk loci defined by LOAD GWAS (Neuner et al., 2019a). The AD-BXD panel has been used to nominate several resilience factors based on 'omics' analysis of strains stratified as resilient or susceptible to cognitive decline in the presence of pathology (Heuer et al., 2020; Neuner et al., 2019b). While progress has been made, there is still a need to identify and prioritize additional human-relevant resilience factors to advance drug interventions to pre-clinical studies. By harmonizing molecular signatures of resilience in this mouse model panel with those found in humans, we establish a framework to

nominate translationally-relevant resilience candidates that can undergo further testing in pre-clinical studies.

In this study, we integrated cortical transcriptomic data from the human ROSMAP and the mouse AD-BXD cohorts and discovered that cognitive resilience to AD is associated with the upregulation of gene expression in a subset of excitatory neurons. We identified biological processes such as axonal and dendritic growth, regulation of action potential, and protein production as enriched in the signature gene list. We further narrowed down the list of candidate genes via validation in orthogonal human data sets and nominated resilience targets, including *ATP1A1*, *GABRB1*, *PTK2*, and *ROCK2* based on their high potential for drug targetability. Thus, we demonstrate the power of cross-species transcriptomic analyses to identify novel AD resilience factors.

Methods

Mouse subjects

The AD-BXD panel of mice were generated as previously described (Neuner et al., 2019a). Briefly, female 5XFAD mice on C57BL/6J background harboring five human mutations that cause familial AD (Stock No: 34848-JAX; B6.Cg-Tg(APPSwFlLon,PSEN1*M146L*L286V)6799Vas/Mmjax) were mated with males from the BXD panel (Ashbrook et al., 2021; Peirce et al., 2004; Taylor et al., 1999). The resulting F1 mice were group-housed (2-5 mice/cage) in a facility with a 12-hour light and dark cycle and had free access to food and water. Only female mice were used in this study. Mouse studies were carried out at the Jackson Laboratory and the University of Tennessee Health Science Center and were approved by the Institutional Animal Care and Use Committee (IACUC) at each

location. All animal studies were conducted in compliance with the National Institutes of Health Guidelines for the Care and Use of Laboratory Animals.

Contextual fear conditioning

Mice were trained on contextual fear conditioning (CFC) paradigm as reported previously (Neuner et al., 2016; Neuner et al., 2019a; Neuner et al., 2015b). After three days of habituation to transport and to the testing room, the mice were placed in a testing chamber. After a brief baseline period (150-180 s), four mild foot shocks (1 second, 0.9 mA) separated by 115±20 seconds were applied. Contextual fear memory (CFM) was measured 24 hours later by placing the mouse in the same testing chamber and measuring percent freezing during a 10-minute time period. Female AD-BXDs and their non-transgenic littermates were tested on CFC at 6 and 14 months of age.

Selection of strains for transcriptomic analyses

We analyzed a group of 14 strains, including two founder strains (B6*B6 and B6*D2 F1s) that differed in CFM at 14 months. Strains were stratified into resilient and susceptible based on population mean. AD-BXD strains were 28, 33, 39, 50, 53, 65, 66, 83, 99, 113, 124, 161, and the B6 and B6*D2 founder strains, along with the non-transgenic counterparts to all 14 strains. To select samples that were most representative in terms of CFM for snRNA-seq analyses, samples from mice nearest the strain average of CFM value (where available) were selected for each strain at 6 (mature) and 14 (middle-aged) months of age for both 5XFAD and their non-littermate controls, resulting in 56 total samples. Quality control was performed on snRNA-seq data as follows: samples that were below 2.5 standard deviation of median genes per nucleus, total genes detected, and median UMI counts were replaced with samples from a mouse with the same demographics (strain, age, 5XFAD mutation status). This resulted in three samples needing to be replaced. Mean ages with standard deviation for each group were as follows:

mature adult mice: 5.96 ± 0.44 months for transgenic animals; 6.00 ± 0.49 months for non-transgenic animals; middle-aged mice: 13.98 ± 0.28 for transgenic animals; and 13.92 ± 0.41 months for non-transgenic animals (n = 14 for each group, and n = 7 for cognitively impaired and unimpaired within each group) (Fig. 1A).

Stratifying mouse populations based on memory performance

To define resilient and susceptible groups, transgenic mice at 14 months of age were ranked according to their individual CFM performance as reported previously (Neuner et al., 2019a) (Fig. 1B). Mice that performed below average were classified as susceptible, and mice that performed above average were classified as resilient (Fig. 1B).

RNA sequencing for mouse subjects

Mice were anesthetized with isoflurane and decapitated after CFM testing. The brains were removed and dissected after olfactory bulbs removal. RNA was isolated from snap-frozen frontal cortex (anterior to the anterior forceps of the corpus callosum) samples from one hemisphere using Nuclei Isolation Kit: Nuclei EZ Prep (Sigma-Aldrich Cat. No. NUC-101). Briefly, 50 µl of EZ Lysis Buffer and RNase inhibitor (1000 units/mL; Protector RNase Inhibitor, MilliporeSigma Cat. No. 03335399001, 2000 U, 40 U/µL) were added to 1.5 mL DNA LoBind tubes (Eppendorf Cat. No. 022431021) containing brain tissue. Tissue was ground with Bel-Art Disposable Pestle (Sigma Aldrich Cat. No. BAF199230000). The tissue was washed off from the pestle with 25 µl of Lysis Buffer, and the tube was placed on ice for 5 minutes. The sample was centrifuged at 500xg for 5 minutes at 4 °C. Supernatant was removed and the pellet was resuspended in 50 µL of Lysis Buffer using a wide bore tip. The sample was placed on ice for 5 minutes, after which 50 µl of PBS containing 0.04% BSA (from LAMPIRE Biological Laboratories Cell Culture Grade 35% BSA Liquid (Fisher Scientific Cat. No. 50-414-159) and RNase inhibitor (40 units/mL) were added. The sample was centrifuged for 5 minutes at 4 °C at 500xg. Thereafter,

the sample was resuspended in 100 µl of PBS containing 0.04 % BSA and RNase inhibitor and pushed through a pre-wet 40 µm filter (PluriStrainer Mini 40 µm Cell Strainer (Pluri Select Cat. No. 43-10040-60)). The sample was centrifuged for 5 minutes at 4 °C at 500xg, and resuspended in 100 µl of PBS containing 0.04% BSA and RNase inhibitor, then pushed through a pre-wet 5 µm filter (PluriStrainer Mini 5 µm Cell Strainer, (Pluri Select Cat. No. 43-10005-60). After a final centrifugation step at 500xg for 5 minutes at 4 °C, the sample was resuspended in 1000 µL of PBS containing 0.04% BSA and RNase inhibitor and immediately processed as follows.

Nuclei quality was assessed via brightfield imaging and counted via Trypan Blue and a Countess II automated cell counter (ThermoFisher), and up to 12,000 nuclei were loaded onto one lane of a 10X Chromium Controller. Single nuclei capture, barcoding and library preparation were performed using the 10X Chromium platform (Zheng et al., 2017) version 3 chemistry and according to the manufacturer's protocol (#CG00052). cDNA and libraries were checked for quality on Agilent 4200 Tapestation, quantified by KAPA qPCR, and pooled at 33.33% of an Illumina NovaSeq 6000 S2 flow cell lane, targeting 6,000 barcoded nuclei with an average sequencing depth of 100,000 reads per nuclei.

Illumina base call files for all libraries were demultiplexed and converted to FASTQ files using Illumina bcl2fastq 2.20.0.422. A filtered digital gene expression matrix was generated for each gene expression library against the 10X Genomics mm10 reference build (version 3.0.0, GRCm38.93 including introns for pre-mRNA mapping) using 10X Genomics CellRanger count version 3.1.0 for all samples.

Single nucleus RNA-seq data for human subjects

As described in the original report (Cain et al., 2020), frozen dorsolateral prefrontal cortex (DLPFC) brain tissue was profiled for snRNA-seq using 10X Chromium version 2 chemistry for

24 ROSMAP individuals, with six donors per group (three male and three female) from four categories: cognitively normal with low AD pathology, cognitively normal with high AD pathology (resilient), cognitively impaired with low AD pathology, cognitively impaired with high AD pathology (susceptible) (Fig. 1A). General QC measures are described in the original study, and all data is available on the AD Knowledge Portal hosted on Synapse.

Mouse data set preparation

The mouse data set was combined from individual files using Seurat package (Hao et al., 2021; Stuart et al., 2019) in R (R Core Team, 2021), with features retained when expressed in at least 10 nuclei and nuclei kept with at least 200 features. Then, nuclei with mitochondrial, ribosomal, and pseudo-genes over 5 % and RNA count below 500 or above 20,000 were excluded. Thereafter, all mitochondrial genes were removed. The data set was batch corrected on sequencing date using harmony package (Korsunsky et al., 2021) with 30 dimensions and resolution of 0.5. Doublet check was performed with 5 % rate using DoubletFinder R package (McGinnis et al., 2019). According to pre-set thresholds, three clusters with doublet rates of over 40% and one cluster with under 100 nuclei were removed from further analysis, resulting in 36 clusters for 26,006 genes by 186,900 nuclei.

Human data set preparation

The raw human gene counts and the metadata (Cain et al., 2020) were re-processed to ensure same treatment as the mouse data set. The human data set was taken through an identical pipeline as the mouse data set, with two modifications. One, an additional first step of removing duplicated genes after summing counts was done. Two, no batch correction was performed. According to the pre-set thresholds, one cluster with both high doublet rate and fewer than 100 nuclei was removed, resulting in 22 clusters for 26,805 genes by 168,282 nuclei.

Integration of Datasets

An average of 7,012 and 3,338 nuclei per sample for human and mouse samples, respectively was obtained after filtering and quality control steps, totaling 168,282 human and 186,900 mouse nuclei.

Gene name translation. Mouse gene names were converted into homologous human gene names using curated and publicly available, published data sets consisting of 17,629 gene names (Hart, 2019; Xu et al., 2020), resulting in a mouse data set of 16,537 genes by 186,900 nuclei. Raw human and mouse data were extracted from processed objects for integration.

Optimization and Integration. To select lambda and k parameters, lambda optimization was run for k = 20, 25, 30, while k optimization was done with lambda set to 15, 20, and 30 (Fig. 1S A and B). For final analyses, the choice was lambda = 30 and k = 20, 25, 30. LIGER (Welch et al., 2019) with R package rliger (Welch et al., 2021) was used to integrate raw human and mouse data processed as described above, with 2,000 variable genes, lambda = 30, k = 20, 25, 30, with 3 restarts and maximum iteration of 100. After quantile normalization and UMAP (Uniform Manifold Approximation and Projection) dimension reduction for visualization (Fig. S1 C), alignment and agreement were calculated, and the object was converted to Seurat for downstream analyses. Overall alignment and agreement metrics were: 0.7152 and 0.0199, 0.7557 and 0.0298, 0.7193 and 0.0324 for k = 20, 25, and 30, respectively. Integrated object with highest alignment metric, k=25, was chosen for downstream analyses (with individual cluster alignments in Table S1).

Integrated dataset analyses

Cell type identities for each cluster in the integrated data set were assigned using a combination of R package MetaNeighbor (Crow et al., 2018) and differential gene expression analysis (Cain et al., 2020). Reference data set previously trained on the Brain Initiative Cell Census Network (BICCN) mouse primary motor cortex data sets was utilized in MetaNeighbor as previously

described (Fischer et al., 2021) to determine best cell type match for each cluster. The AUROC (area under the receiver operator characteristic curve) was calculated for each cluster, with an average of 0.86 ± 0.10 for highest AUROC (Table S2). Neuronal clusters were classified as excitatory or inhibitory based on SLC17A7/SLC17A6, and GAD1/GAD2 expression, respectively.

Differential gene expression analyses

Differential gene expression analysis was performed on human and mouse samples separately. For analysis of resilience signatures, genes that were expressed in at least 10% of nuclei in least one group (resilient or susceptible) were analyzed in the data from 14-month-old transgenic mice and human subjects with high pathology. Differential expression statistics for each cluster were performed with glmmTMB function (Brooks et al., 2017) that uses generalized linear mixed model (GLMM) using Template Model Builder (TMB) with family function nbinom2(link = "log") with cognition status (resilient or susceptible) as fixed effect and with each individual as the random effect, and ANOVA function in the car package (Weisberg, 2019). Multiple testing adjustment was calculated for each cluster with the Benjamini–Hochberg procedure using p.adjust function of the stats package in R (R Core Team, 2021). Upregulated and downregulated genes were those whose $\log_2$FC is equal to or greater than 0.25, or equal to or less than -0.25, respectively. Gene ontology (GO) (Ashburner et al., 2000; Gene Ontology, 2021) enrichment analysis on upregulated or downregulated genes was performed with clusterProfiler package with all gene set sizes and against all background genes for broad categories, and using gene sizes of under 500 for sub-classification (Wu et al., 2021).

For analysis of resilience genes, the same generalized linear mixed model analysis as above was performed on pre-selected candidate genes in four groups: 6-month-old non-transgenic mice, 14-month-old non-transgenic mice, 6-month-old transgenic mice, and 14-month-old transgenic mice.

Immunohistochemistry

The immunohistochemistry study incorporated a different cohort of male and female 14-month-old AD-BXD mice from the following strains: 14, 16, 22, 32, 44, 55, 56, 60, 61, 66, 68, 75, 77, 81, 87, 89, 99, 100, as well as the B6 and D2 F1s. For the female-only dataset, samples from the following AD-BXD strains were included: 14, 16, 22, 55, 75, 77, 81, 99, as well as the B6 and B6*D2 F1s. After CFM testing, mice were anesthetized with isoflurane and decapitated. The brains were removed and halved; one hemibrain was placed in 4% paraformaldehyde and kept at 4°C until the samples were sent to Neuroscience Associates (NSA, Knoxville, TN) for processing. The hemibrains were embedded, processed, and stained simultaneously in blocks of 40. The brains were freeze-sectioned coronally at 40 µm intervals (not including the cerebellum). Serial sections were stained for neurons using NeuN (anti-NeuN antibody, clone A60, biotin conjugated, Millipore Cat. No. MAB377B, 1500 dilution) and visualized using 3,3′-Diaminobenzidine (DAB), resulting in 22 images per brain on average. Images were taken with 20x objective on a Huron Digital Pathology TissueScope LE120 (0.4 microns/pixel).

Image analysis

Cropped and down-sampled images from hemibrains of 29 mice were systematically registered to the Allen Brain Atlas CCFv2017 (Wang et al., 2020) and NeuN coverage across layers 4 and 5 of designated cortical regions were quantified using the QUINT workflow (Berg et al., 2019; Groeneboom et al., 2020; Yates et al., 2019). Neuronal coverage in these regions was assessed as a measure of the area of stain coverage over the area of the region. Regions of the frontal cortex were identified and neuronal coverage within layers 4 and 5 were averaged from all sections per brain. Layers 4 and 5 from the following areas of the frontal cortex were assessed: prelimbic area, infralimbic area, anterior cingulate area (dorsal part), anterior cingulate area, anterior cingulate area (ventral part), agranular insular area (dorsal part), agranular insular area (ventral part), primary motor area, secondary motor area, primary

somatosensory area, somatosensory areas, orbital area (lateral part), orbital area (medial part), dorsal peduncular area, and frontal pole.

Resilient and susceptible status for each strain was assigned using CFM averages across the male and female 14-month-old AD-BXD data set (Neuner et al., 2019a). Strains that fell below the population average were deemed susceptible while those scoring above the average were deemed resilient to cognitive decline. Cognitive status was then correlated with strain averages of neuronal coverage from each layer 4 and 5 frontal cortical region using a biserial correlation.

Human references validations

To evaluate the relevance of resilience candidates to resilience in independent human cohort studies, our team leveraged published genomic, transcriptomic, and proteomic data. Both human and mouse genes were evaluated, with reported values for mouse genes included in this report. First, we leveraged data from a published genome-wide association study (GWAS) of resilience to AD neuropathology, defined as better-than-predicted cognitive performance given an individual's amyloid burden (Dumitrescu et al., 2020). PrediXcan (Gamazon et al., 2015) was used to quantify predicted levels of *ZCCHC17* expression leveraging the GTEx database for model building and applied using GWAS data. Tissue-specific expression models were built leveraging elastic-net regression in the cis gene region (within 1Mb) and selected based on five-fold cross-validation as previously described. We then regressed our published resilience trait (n=5108) on each gene model covarying for age and sex. Correction for multiple comparisons was completed leveraging the false discovery rate (FDR) procedure (correcting for all gene-tissue combinations).

Next, we leveraged bulk transcriptomic data from the ROSMAP to evaluate whether the expression of resilience genes also related to cognitive performance in the years preceding death. ROSMAP enrolled older adults without dementia who agree to annual clinical evaluations

and brain donation at death (Bennett et al., 2018). Bulk RNA sequencing was performed in 3 brain regions: the head of the caudate nucleus (CN), dorsolateral prefrontal cortex (DLPFC), and posterior cingulate cortex (PCC), all of which were processed following a published protocol (Wan et al., 2020). A global cognitive composite was calculated by averaging z-scores from 17 tests, as previously described (Wilson et al., 2015). We evaluated transcript associations with cross-sectional cognition covarying for age at death, post mortem interval, and sex, and we evaluated associations with longitudinal cognition leveraging mixed effects regression models with the same covariates and both the intercept and slope (years from death) entered as fix and random effects in the model. Correction for multiple comparisons was completed with FDR procedure.

Then, we assessed whether identified genes were associated with resilience in ROSMAP focusing on the cell-type identified in mouse discovery analyses (excitatory neurons). We leveraged published snRNA data from ROSMAP (Mathys et al., 2019) comparing resilient (i.e., pathology confirmed AD but cognitively normal) to path confirmed AD (i.e., pathology confirmed AD and clinical dementia). As described previously, single nuclei were isolated from frozen DLPFC for 48 ROSMAP samples and sequenced using droplet-based snRNA-seq. Expression values were normalized and clustered into 20 pre-clusters. We focused on the excitatory neuron cluster for this analysis. Differential expression was evaluated leveraging the Wilcoxon Rank Sum test and correction for multiple comparisons was completed with the FDR procedure.

Finally, to identify proteins that shared resilience signatures in the human ROSMAP and Banner data set, data from Johnson et al. (Johnson et al., 2022) was used (Supplementary Table 6, considering p- and bicor values for MMSE30). Proteins that were upregulated in AsymAD vs AD can be found in Supplementary Table S2 of that publication. For both data sets, in cases where multiple values were reported per protein, the proteins with the lowest *p*-values were chosen.

Druggability rankings

Druggability of nominated genes were assessed using a protein druggability dataset (https://www.synapse.org/#!Synapse:syn13363443) combined with Agora AD gene nomination (https://agora.adknowledgeportal.org/genes). R package biomaRt was used to match gene names with their ensembl IDs (Durinck et al., 2005; Durinck et al., 2009).

Small molecules targeting genes of interest were identified using https://www.genecards.org/ resource.

Statistical analysis and software

For Fig. 2A, R package corrplot (Simko, 2021) was used on log of average expression + 1. Correlation values for Fig. 2 B were calculated and graphed with stat_poly_eq() function from R package ggpmisc (Aphalo, 2021) on genes with expression in at least one of the groups.

For Fig. 3A and B, cluster frequencies were calculated with all four groups; then, R package rstatix (Kassambara, 2021) was used to compare resilient and susceptible groups, t-test was performed for each cluster within each species, with Benjamini-Hochberg multiple comparison correction.

For Figs. 4 and S3, cognitive status of strains based on strain average CFM (resilient or suspectable) was correlated with strain averages of neuronal coverage from each of the layers 4 and 5 in the frontal brain region using a biserial correlation. Correlations between regions for the heatmap were run using rcorr from Hmisc in R (Harrell Jr et al., 2021). The correlation between regions and the binary R vs S status was completed using a cor.test (method = pearson) in R.

Results

High alignment of integrated cross-species gene expression profiles enables conserved resilience factor interrogation

We integrated transcriptomic data from human and mouse cohorts to identify conserved cell type-specific signatures of resilience to AD. We used human prefrontal cortex (PFC) tissue samples from the ROSMAP cohort (Cain et al., 2020), which includes tissue from a number of resilient and susceptible individuals, as well as cognitively normal controls (Fig. 1A). For mouse, we used frontal cortex tissue samples containing PFC from AD-BXD strains determined to be cognitively resilient and susceptible to the presence of the 5XFAD transgene (Fig. 1B), along with their non-transgenic genetically identical counterparts (Fig. 1A).

Integration of processed data (Fig. 1A) resulted in an integrated space with a high overall alignment score of 0.76 (comparable to examples in Welch et al 2019), with individual cluster alignments that ranged from 0.47 to 0.92, with mean of 0.74 (Table S1 and Fig. 1C). The majority of clusters had alignment above 0.65, with exceptions of clusters C9 – mixed, C13 - inh. neurons, C25 – endothelial, C12 - immune – microglia, C16 - inh. neurons, and C23 - inh. Neurons, which had lower confidence scores. The lower alignment scores for inhibitory neurons may be indicative of tissue dissection in mouse including subcortical regions. There was also comparable representation of human and mouse nuclei in 25 clusters (as observed in cluster proportion composition and individual UMAPs in Fig. 1C). Additionally, all clusters had contributions from human and mouse samples (Fig. S2).

All major cell types were identified in the integrated data set using MetaNeighbor and marker genes: excitatory (clusters 17, 20, and 24) and inhibitory (clusters 5, 13, 15, 16, 22, and 23) neurons, astrocytes (cluster 2, 10, and 21), oligodendrocytes (clusters 6 and 7), oligodendrocyte precursors (OPCs, cluster 4), microglia (clusters 12, 14, and 19), vascular and leptomeningeal

cells (VLMC, clusters 8 and 18), endothelial cells (clusters 1 and 25), and pericytes (cluster 3) (Fig. 1D and E, Table S2). Cluster 9 had a mixed cell signature and was labeled as a “mixed cluster” (Fig. 1E, rightmost cluster). The ratio of cell types across samples was proportionally similar (Fig. 1F). Additionally, we observed high correlation values within each cluster for human vs mouse when gene expression in each cluster was correlated between species (Fig. 2A and B, top and center), with lower correlation between clusters assigned to different cell types (Fig. 2A and B, bottom). We also confirmed cell type cluster assignment using marker genes when the data were separated by species (Fig. 2C). Note that because the mouse gene names were converted to their human equivalent, when describing the mouse portion of results from the integrated data analysis, the names were left in all capitals. When the mouse results were considered separately, homologous mouse gene names were used.

Gene upregulation in excitatory neurons is the strongest resilience signature

Resilience may arise due to broad changes in cellular composition, changes in gene expression, or a combination of both. Thus, to probe the nature of resilience in the AD-BXD population, we analyzed whether resilience is associated with differences in cellular composition and/or gene expression. We found that there were no statistically significant differences in cluster composition between resilient and susceptible individuals in the human cohort and in the 14-month-old AD-BXDs (Fig. 3A and B). This suggests that changes associated with resilience are subtle, leading us to hypothesize that the differences in long term memory between resilient and susceptible individuals may be reflected in altered gene expression in one or more cell types, and/or changes in the proportion of nuclei expressing a set of genes within one or more cell types.

Overall, there were 124 human and 282 mouse genes across all clusters that were differentially expressed between resilient and susceptible groups (see Methods, adjusted p-value ≤ 0.05 and $\log_2$FC ≥ 0.25 or ≤ -0.25) (Fig. 3C and D), with no overlap between species, with most of the differentially expressed genes present in neuronal clusters (Fig. 3E and F). Excitatory neuronal cluster 20, annotated as Layer 4/5 intratelencephalic (IT) neurons using MetaNeighbor (Table S2), contained most of the genes that were significantly differentially expressed in both the mouse and the human subsets (Fig. 4A and B).

To test the hypothesis that cognitive status was not associated with differences in neuronal composition suggested by comparable relative proportions of nuclei in susceptible and resilient AD strains (Fig. 3A), we quantified the coverage of NeuN positive cells in layers 4 and 5 of the frontal cortex in a separate cohort of AD-BXD mice by immunohistochemistry (IHC). We found that cognitive status was not correlated with regional differences in NeuN load in a population of male and female 14-month-old AD-BXDs. This lack of relationship between neuron coverage within layers 4 and 5 of the frontal cortex and resilient versus susceptible status suggests that gross changes in neuronal cell composition are unlikely to be driving the differences in CFM among the strains assessed (Figs. 4C and S3). The same was found when analyzing the female subset of mice; there was no significant association across all frontal cortical regions measured except in the orbital area, medial part, layer 5 NeuN (*p*-value 0.004), but it did not survive FDR correction (*p*-value 0.1) (data not shown). Therefore, since we observed no change in neuron load by nuclear fraction (Fig. 3B) and IHC analyses (Fig. 4C). We interpret this as cognitive resilience is conferred, in part, by changes in gene expression levels in layer 4/5 neurons, as there is no observable difference in the degree of neurodegeneration between susceptible and resilient individuals using two orthogonal analyses.

Notably, differentially expressed genes were overrepresented in excitatory neuronal cluster 20. Specifically, our analysis identified 39 human and 196 mouse genes with greater mean and

percent nucleus expression in resilient individuals, indicating upregulation may be driven by more neurons expressing these genes. The 196 upregulated mouse genes were not significantly differentially expressed in animals from the corresponding non-transgenic strains at 6 or 14 months or the transgenic animals at 6 months, suggesting that genes are activated in response to the presence of amyloid and increasing age in resilient strains.

When we compared GO enrichment analyses on human and mouse gene sets from all clusters, we found that of the two species, only mouse gene GO terms reached significance for biological processes (GO:BP), including neurogenesis, nervous system development, viral processes, cellular protein localization, and mRNA metabolic process (Fig. 4D, far left). For molecular function enrichment, the human gene set list was enriched only for prostaglandin-E synthase activity, while the mouse gene set list was enriched in multiple binding categories, such as protein, RNA, and enzyme binding (Fig. 4D, middle). While there was overlap in general categories of cellular compartments enriched, only mouse genes were enriched for neuron-specific compartments, such as synapse and neuron projection (Fig. 4D, far right). The singular enriched human GO molecular function or biological process pathways is likely due to the fact that there are fewer differentially expressed genes, and poorer gene coverage from the Chromium v2 library for the human compared to the v3 library for the mouse indicated by more reads per nucleus on average in each cluster for mouse than human (mean of average counts per nucleus in each cluster: $\bar{x}$ = 0.146 counts, sd = 0.090 counts for mouse; $\bar{x}$ = 0.047 counts, sd = 0.019 counts for human). Additionally, other factors such as longer post-mortem interval during human brain sample collection, as well as the general diversity of human samples due to cumulative lifetime exposure and experiences, may contribute to variability. Since the mouse data set had a greater read depth, we examined the resilience mouse gene list to select resilience transcriptomic candidates from the 14-month-old transgenic cohort in the next sections of this report. Because of the high alignment of human and mouse transcriptional

profiles, we hypothesize that the translational relevance of the mouse resilience findings is high, which we test directly in orthogonal human data sets, below.

Resilience gene candidates involved in diverse biological pathways

Some of genes among the highest ranked top 5 biological processes (mRNA metabolic process, nervous system development, neurogenesis, viral process, and cellular protein localization) share pathways (Fig. 5A). For example, gene *NCKAP1* is in the categories nervous system development, neurogenesis, and viral process, while gene *NEDD4L* is in the categories nervous system development, neurogenesis, viral process, and cellular protein localization. As well, *ROCK2* and *RPL* and *RPS* genes (*RPL26*, *RPL28*, *RPL3*, *RPL5*, *RPS23*, *RPS3A*, *RPS7*) share categories of cellular protein localization, mRNA metabolic and viral processes. This pleiotropy, as well as the presence of genes that have not been implicated in the nervous system development directly, reveals new potential functions of these genes in neurons, as some of these genes and their protein products may have been previously studied in non-neuronal contexts. Note that gene names were left in the human notation (all letters capitalized) due to the use of human annotations for GO analysis.

Notably, neurogenesis pathway (GO: 0022008) is a top 5 pathway with 40 genes (e.g. *NTRK2*, *MAP2*, *GRID2*, *MACF1*, *RTN4*). Although neurogenesis has been most extensively studied in the hippocampus and the subventricular zone, it has also been observed in multiple other regions in rodent studies (Jurkowski et al., 2020). While the degree to which neurogenesis is present in the adult human hippocampus remains highly controversial (Franjic et al., 2022; Moreno-Jimenez et al., 2021; Sorrells et al., 2021), it has been shown to be decreased in neurodegenerative diseases (Terreros-Roncal et al., 2021) and associated with cognition (Tobin et al., 2019). We observed enrichment of these genes in these resilient cases, although all

these genes are also part of the nervous system development process (Figs. 5A and S4) because neurogenesis GO term is a child of the nervous system development GO term (GO:0007399). Additional analyses revealed low expression of neurogenesis markers observed in other studies, e.g. *Dcx*, *Mki67*, *Mcm2*, *Lpar1*, *Pax6* and *Sfrp1* (Ayhan et al., 2021; Sorrells et al., 2021; Zhong et al., 2018) (Fig. S5). We observed *Dcx* in inhibitory neurons (Fig. S5), as previously described in the hippocampus (Franjic et al., 2022). Thus, it remains unsettled whether or not the resilience signature in excitatory neuronal cluster 20 is truly indicative of newly born neurons in the cortex.

To further understand known neuronal gene functions associated with resilience in our study, we further classified genes under the broad term “nervous system development”. More specific roles for genes were uncovered, including regulation of neuron differentiation (*BCL11B*, *CSNK1E*, *NCOA1*, *OPA1*, *PCP4*, *TCF4*, *ZNF536*), axonogenesis (*BCL11B*, *KIF5B*, *MACF1*, *MAP2*, *MYCBP2*, *NFIB*, *NTRK2*, *PTK2*, *PTPRA*, *RTN4*, *SPTBN1*), myelination (*ADAM22*, *CLU*, *HEXB*, *MAL*, *NTRK2*, *SIRT2*, *TPPP*), regulation of membrane potential (*ATP1A2*, *GABRB1*, *GRID2*, *GRIN2A*, *KCNIP2*, *KIF5B*, *NEDD4L*, *NTRK2*, *PRKCZ*, *RGS4*), dendrite morphogenesis (*CAMK2B*, *IL1RAPL1*, *MAP2*, *NEDD4L*, *OPA1*, *WASL*), and regulation of amyloid-beta formation (*CLU*, *LRRTM3*, *NTRK2*, *RTN4*) (Fig. S6). These findings add to the growing body evidence that resilience is associated with improved neuronal function (Neuner et al., 2022). Yet, how transcriptomic upregulation of these genes translates to improved cognition remains to be discovered.

Many genes in the broad category “viral process” (28 genes) that we identified to be upregulated in resilient mice have known functions in the protein life cycle. More narrowly defined enriched pathways include viral transcription, RNA catabolic process, and SRP-dependent cotranslational protein targeting to membrane (Fig. S7). Ribosomal protein small and large genes (*RPL26*, *RPL28*, *RPL3*, *RPL5*, *RPS23*, *RPS3A*, and *RPS7*) are involved in multiple

biological process pathways in the protein life cycle, such as translational initiation, cotranslational targeting of proteins to membrane, as well as catabolic processes (Fig. S7). Other genes involved in catabolic process are *PSMA7* (Proteasome 20S Subunit Alpha 7) and *PSMC3* (Proteasome 26S Subunit, ATPase 3), both of which have roles in degrading RNA and proteins, which is essential to maintain homeostasis. Genes categorized as involved in viral transcription include *CCNT2* (Cyclin T2) with known function in cell cycle and cell division and previously shown to be involved in HIV and breast cancer, and *TPR* (Translocated Promoter Region, Nuclear Basket Protein) involved in mRNA export from the nucleus and cell division. The fact that these genes were upregulated in resilient individuals may mean that protein machinery is engaged to upregulate other genes potentially involved in resilience. On the other hand, this process may also be associated with improved general protein synthesis in resilient individuals. In other studies, protein synthesis was impaired in patients with mild cognitive impairment (MCI) and AD due to ribosomal dysfunction (Ding et al., 2005), and expression of multiple RPS and RPL genes was dysregulated in AD, with examples of genes in our study - *RPL26* downregulated in DG and CA1 of late stage AD, and expression of *RPL5* increased in CA1 late stage AD (Hernandez-Ortega et al., 2016). In an animal model, ribosomal protein levels were also dysregulated, with both *RPS23* downregulated in temporal lobe and *RPL28* downregulated in hippocampus of APP/PS1 mice (Wang et al., 2019). Moreover, the function of translation accuracy of RPS23 was demonstrated to be related to longevity (Martinez-Miguel et al., 2021). As well, *USP15* (Ubiquitin Specific Peptidase 15) and *UBC* (Ubiquitin C) are in the ubiquitin pathway. Among other candidates in the broad “viral processes” pathway that have been implicated in neuronal function include Cul5, which is involved in neuron migration (Simo et al., 2010), TSPAN7 (Tetraspanin 7), with a key role in establishing morphology of neurons and synaptic function (Bassani et al., 2012), and Pcx (homolog of PC), which was found to maintain neuron’s oxidized state and prevent cell death (Motori et al., 2020). Overall, the

upregulation of these genes involved in production and maintenance of proteins and the cell cycle in resilient individuals points to overall improvement of neural function.

The remaining two pathways – “cellular protein localization” and “mRNA metabolic processes” have many overlapping genes with the previously discussed pathways and provide further evidence of biological processes likely involved in resilience. For instance, investigating smaller pathways for genes in “cellular protein localization” category reveals many overlapping pathways in the top 10 with “viral processes” category, such as protein targeting to membrane and ER, and a new pathway of targeting to the periphery (*CLASP2*, *EFR3A*, *MACF1*, *GRIN2A*, *KIF5B*, *ADAM22*, *PRKCZ*, *DPP10*, *SPTBN1*, and *ROCK2)* (Fig. S8). Among genes in this broad category or their protein products, many have known roles in neuronal function as well, such as CLASP2, with a role in correct neuronal layering in development (Dillon et al., 2017) (in same Reelin pathway as Clu5 mentioned above), HSPA/Mortalin, whose overexpression protected axons (Ferre et al., 2021), and Smg6, with a role in stem cell differentiation (Li et al., 2015) and neurogenesis (Guerra et al., 2021). As well, *TOM1L2* was identified as a causal gene in AD (Ou et al., 2021). Similarly, smaller categories for biological processes among genes in the broad category “mRNA metabolic process” reveals shared pathways with “viral processes”, such as RNA catabolic process (*RPS* and *RPL* genes, *PSMD14*, *AGO3*, *SMG6*, *PUM2*, *CNOT4*, *PSMA7*, *PSMC3*, *UBC*, *ROCK2*) (Fig. S9). Two other pathways involved in RNA include “RNA splicing” (*RBM5*, *DDX17*, *PSIP1*, *CELF3*, *DDX42*, *PUF60*, *ZC3H13*, *TRA2A*, *LUC7L2*, *LUC7L3*, *SRSF7*, *SRPK1*) and “ribonucleoprotein complex biogenesis” (*RBM5*, *DDX17*, *PSIP1*, *CELF3*, *AGO3*, *PUF60*, *LUC7L2*, *LUC7L3*, *RPL3*, *RPL5*, *RPL26*, *RPS7*, *SRPK1*) (Fig. S9). Overall, biological processes pathways enriched in these genes point to ramping up the membrane protein production by upregulating processes involved in RNA production and degradation, as well as ensuring protein localization to correct compartments.

Resilience candidates are upregulated in excitatory neurons and correlate with cognition in independent human reference data sets

We found corroborating evidence of these upregulated mouse genes among several human data sets. Remarkably, when considering expression in excitatory neurons, 101 genes were found to have a significant ($p < 0.05$) increase in expression ($logFC > 0$) in resilient individuals (Table S3) in a ROSMAP cohort (Mathys et al., 2019). In addition, 75 genes were predicted to have differential expression in resilient individuals in various tissues, including the brain, using PrediXcan analysis in GWAS of resilience (Table S4) and expression of 67 genes across three tissues, including the DLPFC, in bulk transcriptomic data were found to be positively correlated with cognition (Table S5).

When considering the products of the 196 genes assessed, 66 proteins with significant positive correlations between protein abundance and MMSE (mini-mental state exam) ($p < 0.05$; higher abundance correlated with better cognition) (Table S6) were identified in the ROSMAP and Banner (Banner Sun Health Research Institute) populations (Johnson et al., 2022). Johnson et al reported that modules “post-synaptic density” and “protein transport” were enriched in proteins correlated with resilience that were previously identified in another study (Johnson et al., 2022). In an analysis that directly compared protein abundance in AD vs AsymAD (individuals with AD pathology and without significant cognitive impairment) (Supplementary Table 2 in Johnson et al), 1,540 proteins had higher abundance in AsymAD ($log2FC > 0$ with adj. p-value < 0.05). Our results enable narrowing down of resilience factors and nomination of cell-type specific targets. In fact, we matched 49 of our gene targets with the protein list, including ATP1A1, ATP1A2, GRIN2A, and ROCK2. Overall, these gene expression and protein data cross-check gives us more confidence that the resilience factors that were identified in the mouse excitatory neuronal cluster 20 from the cross-species integrated data set are translationally relevant.

Nominated resilience candidates include druggable targets

An important factor to consider in nominating targets is whether the gene is druggable. Our study has nominated genes that are targetable based on Agora's druggability criteria (https://www.synapse.org/#!Synapse:syn13363443). After obtaining these data for each gene, we filtered the list by druggability, safety, and accessibility of target. Those genes that are targetable by small molecules, homology, or structure were retained. Of the genes that are targeted by protein structure, only those with two or fewer "red flags" such as it being an essential gene, a cancer driver, having high off target gene expression, or a "black box warning" (label put on by the U.S. FDA to warn about serious safety risk) on drugs currently used in the clinic, were retained. Finally, we arrived at a list of 40 targetable genes (Table S7), nine of which are targetable by small molecules and have a favorable safety profile: *ATP1A1*, *ATP1A2*, *GABRB1*, *KCNH7*, *NISCH*, *PRKCZ*, *ROCK2*, *TUBA1B*, and *JAK1*.

In addition, we reviewed which of the 196 genes had been previously nominated as potential targets for AD. Among the upregulated resilience genes from excitatory neuronal cluster 20, 11 mouse and one human genes have been nominated on Agora by research teams from the NIA-funded AMP-AD consortium (https://agora.adknowledgeportal.org/genes) (Table S8). None of these targets has been validated or are marked for a future validation study. Our data provide new evidence to prioritize these genes for candidate validation: *CLU*, *DPP10*, *DTNA*, *GPM6B*, *GRIN2A*, *KCNJ3*, *MAP2*, *PDHA1*, *PHF24*, *RTN4*, *SLC22A23*, and *ZNF536*.

Discussion

Our findings demonstrate that analysis of integrated mouse and human transcriptomic data uncovers novel and conserved cell type-specific signatures in layer 4/5 cortical neurons

associated with resilience to AD cognitive decline. The integrated approach ensures same treatment of data and allows for straightforward mouse to human comparisons. Using this approach, we identified resilience genes that were confirmed in other human data sets. Specifically, we demonstrated that the majority of cell types resolved from mouse and human snRNA-seq data sets exhibited high alignment, which allowed us to identify translationally-relevant resilience signatures conserved across the two species. We determined that the upregulation of gene expression in layer 4/5 excitatory neuron cluster reflects a robust signature of resilience, while cluster composition remains stable. Through this process, we nominated targeting of specific genes such as *ATP1A1*, *GABRB1*, *PTK2*, and *ROCK2* in pathways such as regulation of membrane potential and axonogenesis in excitatory neurons to promote resilience.

While animal models are necessary for development of AD therapeutics, more translationally-relevant mouse models are needed due to the lack of clinical trial success (De Felice and Munoz, 2016; Oblak et al., 2020). Large-scale efforts to characterize human cohorts and mouse models allows for better understanding of the molecular underpinnings of AD (Gurdon and Kaczorowski, 2021). In particular, several studies reported both shared and divergent signatures between mouse and human transcriptomic AD signatures in microglia and other cell types (Del-Aguila et al., 2019; Hodge et al., 2019; Mathys et al., 2019; Srinivasan et al., 2020). However, many studies share limitations of comparing gene signatures obtained from different computational pipelines, comparing different technology (e.g., snRNA-seq vs scRNA-seq), comparing different brain regions, and only using one or a limited number of genetic backgrounds for mouse models. In our study, we aimed to eliminate several of these technical differences that may confound biological interpretation of results. Therefore, we performed a unified analysis using the same computational pipeline, sequencing technology, and included genetic diversity in profiling a similar region from the mouse and human brain tissue (Fig. 1A). While not all technical differences were eliminated, we demonstrate that this analysis pipeline is

a powerful tool to synthesize transcriptomic data into an interpretable cross-species data set (Fig. 1B-E).

We discovered that while cross-species cluster composition remained unchanged with cognition status (Fig. 3A and B), both human and mouse resilient individuals had an upregulation of genes in one excitatory neuronal cluster (Fig. 4A and B) that was classified as layer 4/5 IT neurons (Table S2). IT neurons are a diverse class of neurons (in terms of connections, activity, and morphology) in layers 2-6 that project to telencephalon and contralaterally (Baker et al., 2018; Harris and Shepherd, 2015). IT neurons in layer 4 process external input, while IT neurons in other layers receive input from L4 and from external sources (Harris and Shepherd, 2015). Some signature genes that have been identified in IT neurons include *Rorb*, *Satb2*, *Pdia5*, and *Gfra* (Baker et al., 2018; Harris and Shepherd, 2015). Interestingly, excitatory neurons expressing RORB were found to be vulnerable in the entorhinal cortex region in human AD (Leng et al., 2021). Targeting excitatory IT neurons in these layers may be a therapeutic strategy to engage resilience mechanisms.

In the approach to targeting excitatory neurons to promote resilience, our data indicate that it is the gene expression that matters, not the survival of neurons. First, we observed that there was no difference in cluster composition (at our optimal cluster resolution) between resilient and susceptible groups (Fig. 3A and B). Second, we corroborated this finding by IHC analysis of NeuN load in layers 4 and 5 of the frontal cortex in the mouse (Figs. 4C and S3). While the 5XFAD mutation itself resulted in a decrease of the number of neurons in layer 5 in middle age mice on C57Bl/6 x SJL and C57Bl/6J backgrounds (Jawhar et al., 2012; Oakley et al., 2006), the difference in neuronal proportions between resilient and susceptible individuals is less clear. In an ROS cohort, same density of neurons was found in AD-resilient (AD pathology and cognitively normal) and AD (AD pathology and dementia) individuals in midfrontal gyrus cortex (frontal lobe) (Arnold et al., 2013). While some coverage analyses show no difference in

neuronal load, they do not take into account brain region shrinkage that is typical in AD. In a study where neurons were counted, fewer neurons were observed in AD patients compared with people with AD pathology but no cognitive symptoms in superior temporal sulcus area (temporal lobe) (Perez-Nievas et al., 2013). In the hippocampus, some regions maintained neuronal numbers while others showed decline between pre-clinical AD (cognitively normal people with AD pathology) and AD in Baltimore Longitudinal Study of Aging and the Johns Hopkins Alzheimer's Disease Research Center cohorts (West et al., 2004).

A closer examination of differentially expressed genes within this IT neuronal cluster revealed potential biological processes of resilience. The broad biological processes of the 196 mouse genes were mRNA metabolic process, nervous system development, neurogenesis, viral process, and cellular protein localization (Fig. 5A). While there were 40 genes in the broad category of neurogenesis, we observed no neurogenesis signature in cluster 20 (Fig. S5). The genes that were labeled as part of the nervous system development were further classified by more specialized categories such as involvement in neuron differentiation, axonal growth, myelination, membrane potential, and dendrite morphogenesis (Fig. S6). Activating these pathways may improve resilience to AD cognitive decline. Additionally, we identified genes in pathways of RNA and protein lifecycle to be upregulated (Figs. S7-S9) and hypothesize that resilient individuals are able to turn on machinery to counteract amyloid pathology after a prolonged assault, as this signature appears late in transgenic animals.

To provide additional evidence of translatability of the resilience genes identified in the mouse, we cross-referenced our findings with a different human cohort of resilient individuals and/or data modality (Johnson et al., 2022; Mathys et al., 2019). Remarkably, we found corroborating evidence among many of the 196 mouse genes in human cohort transcriptional data sets, including upregulation in excitatory neurons of resilient individuals (Table S3), predicted differential expression in resilience in multiple tissues (Table S4), and positive correlation with

cognition (Table S5). As well, we found abundance of about a third of proteins that are products of the resilience genes to be positively correlated with cognition (Table S6).

Finally, in nominating resilience targets we considered the druggablity of these genes. From mining Agora druggability data set, we tabulated targets with the best druggability metrics. From the original list of 196 mouse genes, 11 mouse genes have been nominated on Agora (Table S7), but only *GRIN2A* had a favorable druggability profile, which is why studies such as this are required to nominate more targets. We found 40 additional druggable genes among those that hadn't been previously nominated, including 11 that were validated cross-species in the Mathys et al and Johnson et al data sets (i.e. *ATP1A1*, *CCNT2*, *GABRB1*, *HSPA9*, *MAP2K4*, *MGLL*, *MRAS*, *PPP2R5C*, *PTK2*, *ROCK2*, and *SRPK1*).

To highlight four of these 11 targets, we will discuss *ATP1A1*, *GABRB1*, *PTK2*, and *ROCK2* in some detail. *ATP1A1* (ATPase Na+/K+ Transporting Subunit Alpha 1) codes for one of the four that are catalytic α subunits of Na^+/K^+ ATPase, which is involved in resting membrane potential; its mRNA is expressed in neurons throughout the mouse brain (Murata et al., 2020). *GABRB1* (Gamma-Aminobutyric Acid Type A Receptor Subunit Beta1) is classified by GO:BP as involved in regulation of membrane potential, as well as CNS neuron differentiation and development. *GABRB1* was nominated as an AD risk variant (Neuner et al., 2015a) and has been previously associated with alcohol dependence (Dick and Foroud, 2003) with a suggested role in changing of brain activity in regions of reward processing (Duka et al., 2017). *PTK2* (Protein Tyrosine Kinase 2) (aka *FAK*) is classified under pathways of axonogenesis, cell junction assembly, and regulation of cell morphogenesis, and it was found to be involved in dendrite arborization (Garrett et al., 2012). Interestingly, inactivation of FAK was observed in olfactory bulb of APP/PS1 AD mice, while an activation was observed in LOAD patients (Lachen-Montes et al., 2016). *ROCK2* (Rho Associated Coiled-Coil Containing Protein Kinase 2) plays a crucial role in motor neuron intrinsic excitability (Garcia-Morales et al., 2021). ROCK2 was also characterized

to regulate axonal growth and neuronal death, and, interestingly, it was reported that downregulation is beneficial for neuronal survival (Koch et al., 2014). It was also reported that ROCK2 protein levels are increased in both AD and AsymAD individuals compared to people with no pathology (Herskowitz et al., 2013), and that ROCK2 induced loss of spines in rat hippocampal neurons (Henderson et al., 2019). On the other hand, our analysis of orthogonal human data sets revealed that *ROCK2* had increased expression in excitatory neurons of resilient individuals (Table S3) and levels of ROCK2 to positively correlate with cognition (Table S6). In our mouse snRNA-seq data, these four genes are expressed in at least 10% of nuclei in both groups of mice, with proportionally more resilient nuclei expressing them, while in nuclei that do express the gene, the average expression between resilient and susceptible groups is similar. Therefore, we postulate that upregulating gene expression of these genes in excitatory layer 4/5 neurons may result in improved cognitive resilience.

Small molecules that have been approved for these four genes, listed on genecards.org, include both agonists and antagonists. Focusing on agonists to potentially upregulate cognitive resilience, we identified several potential candidates to test in *in vitro* and animal models. For instance, approved small molecule agonists for *ATP1A1* include magnesium gluconate used for hypomagnesemia (https://go.drugbank.com/drugs/DB13749) and for *GABRB1* include Meprobamate, an anti-anxiety medication (https://go.drugbank.com/drugs/DB00371). On the other hand, approved small molecule inhibitors include for *PKT2* - Fostamatinib, a drug for rheumatoid arthritis (https://go.drugbank.com/drugs/DB12010) and for *ROCK2* - Belumosudil, drug for graft-versus-host disease (https://go.drugbank.com/drugs/DB13931). For drug targets lacking agonists, novel small molecules or gene therapies are needed for validation and pre-clinical studies. Whether targeting these genes specifically in excitatory neurons in layers 4/5 enhances resilience is a topic of future investigations.

It is worth noting that in ROS/MAP and other cohorts, researchers have previously identified factors such as lifestyle and complex traits (Dumitrescu et al., 2020; Negash et al., 2013), pathology burden (Latimer et al., 2019), cellular and structural markers (Arnold et al., 2013; Boros et al., 2017; Perez-Nievas et al., 2013), genes (White et al., 2017; Yang et al., 2020), and proteins (Arnold et al., 2013) associated or correlated with resilience (recently reviewed in (Neuner et al., 2022)). However, proving causality and translating findings to therapeutics remains a challenge. Using the translationally-relevant AD-BXDs, in future studies we aim to study causality, understand the mechanisms of resilience that we nominated in the genetically diverse mouse models, as well as to perform preclinical studies to test top candidates.

In conclusion, our cross-species integrative transcriptomic analyses of individuals resilient to AD cognitive decline resulted in nomination of several resilience targets. The AD-BXD mouse panel allows us to decipher causality and perform mechanistic and pre-clinical animal studies in forthcoming projects.

Acknowledgements

We gratefully acknowledge the contribution of Mike Samuels, Shannon Bessonett, and the Single Cell Biology service, the Genome Technologies service, and Advanced Cyberinfrastructure high performance computing resources at The Jackson Laboratory for expert assistance with the work described in this publication. We acknowledge Stephan Fischer's role in MetaNeighbor studies. The results published here are in part based on data obtained from Agora, a platform initially developed by the NIA-funded AMP-AD consortium that shares evidence in support of AD target discovery (https://agora.adknowledgeportal.org/genes, Site Version 2.2.0-3a1674d, Data Version syn13363290-v33). We are thankful for the funding for this project: R01 AG057914 (C.C.K.); R01 AG054180 (C.C.K); R01 AG075818 (C.C.K.), RF1 AG059778 (C.C.K), Alzheimer's Association Zenith Fellows Award AARF-ZEN-21-846037 (C.C.K. and M.A.T.); R01AG059716 (T.J.H.), R01AG061518 (T.J.H.), R01AG074012 (T.J.H.), R01 AG066831 (V.M.); RF1 AG057473 (V.M.); U54 AG076040 (V.M.); Thompson Family Foundation TAME-AD Award (V.M.); U01AG061357 (N.T.S.); Swiss National Science Foundation fellowship P2EZP3_191873 (S.M.); R01LM012736 (J.G.) and R01MH113005 (J.G.).

Competing interests

T.J.H. serves on the Scientific Advisory Board for Vivid Genomics. All other authors have no competing interests.

References

Aphalo, P.J. (2021). ggpmisc: Miscellaneous Extensions to 'ggplot2'.
Arenaza-Urquijo, E.M., and Vemuri, P. (2018). Resistance vs resilience to Alzheimer disease: Clarifying terminology for preclinical studies. Neurology *90*, 695-703.

Arnold, S.E., Louneva, N., Cao, K., Wang, L.S., Han, L.Y., Wolk, D.A., Negash, S., Leurgans, S.E., Schneider, J.A., Buchman, A.S., *et al.* (2013). Cellular, synaptic, and biochemical features of resilient cognition in Alzheimer's disease. Neurobiol Aging *34*, 157-168.
Ashbrook, D.G., Arends, D., Prins, P., Mulligan, M.K., Roy, S., Williams, E.G., Lutz, C.M., Valenzuela, A., Bohl, C.J., Ingels, J.F., *et al.* (2021). A platform for experimental precision medicine: The extended BXD mouse family. Cell Syst *12*, 235-247 e239.
Ashburner, M., Ball, C.A., Blake, J.A., Botstein, D., Butler, H., Cherry, J.M., Davis, A.P., Dolinski, K., Dwight, S.S., Eppig, J.T., *et al.* (2000). Gene ontology: tool for the unification of biology. The Gene Ontology Consortium. Nat Genet *25*, 25-29.
Ayhan, F., Kulkarni, A., Berto, S., Sivaprakasam, K., Douglas, C., Lega, B.C., and Konopka, G. (2021). Resolving cellular and molecular diversity along the hippocampal anterior-to-posterior axis in humans. Neuron *109*, 2091-2105 e2096.
Baker, A., Kalmbach, B., Morishima, M., Kim, J., Juavinett, A., Li, N., and Dembrow, N. (2018). Specialized Subpopulations of Deep-Layer Pyramidal Neurons in the Neocortex: Bridging Cellular Properties to Functional Consequences. J Neurosci *38*, 5441-5455.
Bassani, S., Cingolani, L.A., Valnegri, P., Folci, A., Zapata, J., Gianfelice, A., Sala, C., Goda, Y., and Passafaro, M. (2012). The X-linked intellectual disability protein TSPAN7 regulates excitatory synapse development and AMPAR trafficking. Neuron *73*, 1143-1158.
Bennett, D.A., Buchman, A.S., Boyle, P.A., Barnes, L.L., Wilson, R.S., and Schneider, J.A. (2018). Religious Orders Study and Rush Memory and Aging Project. J Alzheimers Dis *64*, S161-S189.
Bennett, D.A., Schneider, J.A., Arvanitakis, Z., and Wilson, R.S. (2012a). Overview and findings from the religious orders study. Curr Alzheimer Res *9*, 628-645.
Bennett, D.A., Schneider, J.A., Buchman, A.S., Barnes, L.L., Boyle, P.A., and Wilson, R.S. (2012b). Overview and findings from the rush Memory and Aging Project. Curr Alzheimer Res *9*, 646-663.
Berg, S., Kutra, D., Kroeger, T., Straehle, C.N., Kausler, B.X., Haubold, C., Schiegg, M., Ales, J., Beier, T., Rudy, M., *et al.* (2019). ilastik: interactive machine learning for (bio)image analysis. Nat Methods *16*, 1226-1232.
Boros, B.D., Greathouse, K.M., Gentry, E.G., Curtis, K.A., Birchall, E.L., Gearing, M., and Herskowitz, J.H. (2017). Dendritic spines provide cognitive resilience against Alzheimer's disease. Ann Neurol *82*, 602-614.
Brooks, M.E., Kristensen, K., van Benthem, K.J., Magnusson, A., Berg, C.W., Nielsen, A., Skaug, H.J., Machler, M., and Bolker, B.M. (2017). glmmTMB Balances Speed and Flexibility Among Packages for Zero-inflated Generalized Linear Mixed Modeling. R J *9*, 378-400.
Cain, A., Taga, M., McCabe, C., Hekselman, I., White, C.C., Green, G., Rozenblatt-Rosen, O., Zhang, F., Yeger-Lotem, E., Bennett, D.A., *et al.* (2020). Multi-cellular communities are perturbed in the aging human brain and with Alzheimer's disease. BioRxiv preprint; DOI: 101101/20201222424084.
Crow, M., Paul, A., Ballouz, S., Huang, Z.J., and Gillis, J. (2018). Characterizing the replicability of cell types defined by single cell RNA-sequencing data using MetaNeighbor. Nat Commun *9*, 884.
De Felice, F.G., and Munoz, D.P. (2016). Opportunities and challenges in developing relevant animal models for Alzheimer's disease. Ageing Res Rev *26*, 112-114.
Del-Aguila, J.L., Li, Z., Dube, U., Mihindukulasuriya, K.A., Budde, J.P., Fernandez, M.V., Ibanez, L., Bradley, J., Wang, F., Bergmann, K., *et al.* (2019). A single-nuclei RNA sequencing study of Mendelian and sporadic AD in the human brain. Alzheimers Res Ther *11*, 71.
Dick, D.M., and Foroud, T. (2003). Candidate genes for alcohol dependence: a review of genetic evidence from human studies. Alcohol Clin Exp Res *27*, 868-879.
Dillon, G.M., Tyler, W.A., Omuro, K.C., Kambouris, J., Tyminski, C., Henry, S., Haydar, T.F., Beffert, U., and Ho, A. (2017). CLASP2 Links Reelin to the Cytoskeleton during Neocortical Development. Neuron *93*, 1344-1358 e1345.
Ding, Q., Markesbery, W.R., Chen, Q., Li, F., and Keller, J.N. (2005). Ribosome dysfunction is an early event in Alzheimer's disease. J Neurosci *25*, 9171-9175.
Duka, T., Nikolaou, K., King, S.L., Banaschewski, T., Bokde, A.L., Buchel, C., Carvalho, F.M., Conrod, P.J., Flor, H., Gallinat, J., *et al.* (2017). GABRB1 Single Nucleotide Polymorphism Associated with Altered Brain Responses (but not Performance) during Measures of Impulsivity and Reward Sensitivity in Human Adolescents. Front Behav Neurosci *11*, 24.

Dumitrescu, L., Mahoney, E.R., Mukherjee, S., Lee, M.L., Bush, W.S., Engelman, C.D., Lu, Q., Fardo, D.W., Trittschuh, E.H., Mez, J.*, et al.* (2020). Genetic variants and functional pathways associated with resilience to Alzheimer's disease. Brain *143*, 2561-2575.
Durinck, S., Moreau, Y., Kasprzyk, A., Davis, S., De Moor, B., Brazma, A., and Huber, W. (2005). BioMart and Bioconductor: a powerful link between biological databases and microarray data analysis. Bioinformatics *21*, 3439-3440.
Durinck, S., Spellman, P.T., Birney, E., and Huber, W. (2009). Mapping identifiers for the integration of genomic datasets with the R/Bioconductor package biomaRt. Nat Protoc *4*, 1184-1191.
Ferre, C.A., Thouard, A., Betourne, A., Le Dorze, A.L., Belenguer, P., Miquel, M.C., Peyrin, J.M., Gonzalez-Dunia, D., and Szelechowski, M. (2021). HSPA9/Mortalin mediates axo-protection and modulates mitochondrial dynamics in neurons. Sci Rep *11*, 17705.
Fischer, S., Crow, M., Harris, B.D., and Gillis, J. (2021). Scaling up reproducible research for single-cell transcriptomics using MetaNeighbor. Nat Protoc.
Franjic, D., Skarica, M., Ma, S., Arellano, J.I., Tebbenkamp, A.T.N., Choi, J., Xu, C., Li, Q., Morozov, Y.M., Andrijevic, D.*, et al.* (2022). Transcriptomic taxonomy and neurogenic trajectories of adult human, macaque, and pig hippocampal and entorhinal cells. Neuron *110*, 452-469 e414.
Gamazon, E.R., Wheeler, H.E., Shah, K.P., Mozaffari, S.V., Aquino-Michaels, K., Carroll, R.J., Eyler, A.E., Denny, J.C., Consortium, G.T., Nicolae, D.L.*, et al.* (2015). A gene-based association method for mapping traits using reference transcriptome data. Nat Genet *47*, 1091-1098.
Garcia-Morales, V., Gento-Caro, A., Portillo, F., Montero, F., Gonzalez-Forero, D., and Moreno-Lopez, B. (2021). Lysophosphatidic Acid and Several Neurotransmitters Converge on Rho-Kinase 2 Signaling to Manage Motoneuron Excitability. Front Mol Neurosci *14*, 788039.
Garrett, A.M., Schreiner, D., Lobas, M.A., and Weiner, J.A. (2012). gamma-protocadherins control cortical dendrite arborization by regulating the activity of a FAK/PKC/MARCKS signaling pathway. Neuron *74*, 269-276.
Gene Ontology, C. (2021). The Gene Ontology resource: enriching a GOld mine. Nucleic Acids Res *49*, D325-D334.
Groeneboom, N.E., Yates, S.C., Puchades, M.A., and Bjaalie, J.G. (2020). Nutil: A Pre- and Post-processing Toolbox for Histological Rodent Brain Section Images. Front Neuroinform *14*, 37.
Guerra, G.M., May, D., Kroll, T., Koch, P., Groth, M., Wang, Z.Q., Li, T.L., and Grigaravicius, P. (2021). Cell Type-Specific Role of RNA Nuclease SMG6 in Neurogenesis. Cells *10*.
Gurdon, B., and Kaczorowski, C. (2021). Pursuit of precision medicine: Systems biology approaches in Alzheimer's disease mouse models. Neurobiol Dis *161*, 105558.
Hao, Y., Hao, S., Andersen-Nissen, E., Mauck, W.M., 3rd, Zheng, S., Butler, A., Lee, M.J., Wilk, A.J., Darby, C., Zager, M.*, et al.* (2021). Integrated analysis of multimodal single-cell data. Cell.
Harrell Jr, F.E., Dupont, C., and others. (2021). Hmisc: Harrell Miscellaneous, pp. R package version 4.5-0.
Harris, K.D., and Shepherd, G.M. (2015). The neocortical circuit: themes and variations. Nat Neurosci *18*, 170-181.
Hart, R.P. (2019). Strategies for Integrating Single-Cell RNA Sequencing Results With Multiple Species.
Henderson, B.W., Greathouse, K.M., Ramdas, R., Walker, C.K., Rao, T.C., Bach, S.V., Curtis, K.A., Day, J.J., Mattheyses, A.L., and Herskowitz, J.H. (2019). Pharmacologic inhibition of LIMK1 provides dendritic spine resilience against beta-amyloid. Sci Signal *12*.
Hernandez-Ortega, K., Garcia-Esparcia, P., Gil, L., Lucas, J.J., and Ferrer, I. (2016). Altered Machinery of Protein Synthesis in Alzheimer's: From the Nucleolus to the Ribosome. Brain Pathol *26*, 593-605.
Herskowitz, J.H., Feng, Y., Mattheyses, A.L., Hales, C.M., Higginbotham, L.A., Duong, D.M., Montine, T.J., Troncoso, J.C., Thambisetty, M., Seyfried, N.T.*, et al.* (2013). Pharmacologic inhibition of ROCK2 suppresses amyloid-beta production in an Alzheimer's disease mouse model. J Neurosci *33*, 19086-19098.
Heuer, S.E., Neuner, S.M., Hadad, N., O'Connell, K.M.S., Williams, R.W., Philip, V.M., Gaiteri, C., and Kaczorowski, C.C. (2020). Identifying the molecular systems that influence cognitive resilience to Alzheimer's disease in genetically diverse mice. Learn Mem *27*, 355-371.
Hodge, R.D., Bakken, T.E., Miller, J.A., Smith, K.A., Barkan, E.R., Graybuck, L.T., Close, J.L., Long, B., Johansen, N., Penn, O.*, et al.* (2019). Conserved cell types with divergent features in human versus mouse cortex. Nature *573*, 61-68.

Jawhar, S., Trawicka, A., Jenneckens, C., Bayer, T.A., and Wirths, O. (2012). Motor deficits, neuron loss, and reduced anxiety coinciding with axonal degeneration and intraneuronal Abeta aggregation in the 5XFAD mouse model of Alzheimer's disease. Neurobiol Aging *33*, 196 e129-140.
Johnson, E.C.B., Carter, E.K., Dammer, E.B., Duong, D.M., Gerasimov, E.S., Liu, Y., Liu, J., Betarbet, R., Ping, L., Yin, L.*, et al.* (2022). Large-scale deep multi-layer analysis of Alzheimer's disease brain reveals strong proteomic disease-related changes not observed at the RNA level. Nat Neurosci *25*, 213-225.
Jurkowski, M.P., Bettio, L., E, K.W., Patten, A., Yau, S.Y., and Gil-Mohapel, J. (2020). Beyond the Hippocampus and the SVZ: Adult Neurogenesis Throughout the Brain. Front Cell Neurosci *14*, 576444.
Kassambara, A. (2021). rstatix: Pipe-Friendly Framework for Basic Statistical Tests.
Koch, J.C., Tonges, L., Barski, E., Michel, U., Bahr, M., and Lingor, P. (2014). ROCK2 is a major regulator of axonal degeneration, neuronal death and axonal regeneration in the CNS. Cell Death Dis *5*, e1225.
Korsunsky, I., Millard, N., Fan, J., Slowikowski, K., and Raychaudhuri, S. (2021). harmony: Fast, Sensitive, and Accurate Integration of Single Cell Data.
Lachen-Montes, M., Gonzalez-Morales, A., de Morentin, X.M., Perez-Valderrama, E., Ausin, K., Zelaya, M.V., Serna, A., Aso, E., Ferrer, I., Fernandez-Irigoyen, J.*, et al.* (2016). An early dysregulation of FAK and MEK/ERK signaling pathways precedes the beta-amyloid deposition in the olfactory bulb of APP/PS1 mouse model of Alzheimer's disease. J Proteomics *148*, 149-158.
Latimer, C.S., Burke, B.T., Liachko, N.F., Currey, H.N., Kilgore, M.D., Gibbons, L.E., Henriksen, J., Darvas, M., Domoto-Reilly, K., Jayadev, S.*, et al.* (2019). Resistance and resilience to Alzheimer's disease pathology are associated with reduced cortical pTau and absence of limbic-predominant age-related TDP-43 encephalopathy in a community-based cohort. Acta Neuropathol Commun *7*, 91.
Leng, K., Li, E., Eser, R., Piergies, A., Sit, R., Tan, M., Neff, N., Li, S.H., Rodriguez, R.D., Suemoto, C.K.*, et al.* (2021). Molecular characterization of selectively vulnerable neurons in Alzheimer's disease. Nat Neurosci *24*, 276-287.
Li, T., Shi, Y., Wang, P., Guachalla, L.M., Sun, B., Joerss, T., Chen, Y.S., Groth, M., Krueger, A., Platzer, M.*, et al.* (2015). Smg6/Est1 licenses embryonic stem cell differentiation via nonsense-mediated mRNA decay. EMBO J *34*, 1630-1647.
Martinez-Miguel, V.E., Lujan, C., Espie-Caullet, T., Martinez-Martinez, D., Moore, S., Backes, C., Gonzalez, S., Galimov, E.R., Brown, A.E.X., Halic, M.*, et al.* (2021). Increased fidelity of protein synthesis extends lifespan. Cell Metab *33*, 2288-2300 e2212.
Mathys, H., Davila-Velderrain, J., Peng, Z., Gao, F., Mohammadi, S., Young, J.Z., Menon, M., He, L., Abdurrob, F., Jiang, X.*, et al.* (2019). Single-cell transcriptomic analysis of Alzheimer's disease. Nature *570*, 332-337.
McGinnis, C.S., Murrow, L.M., and Gartner, Z.J. (2019). DoubletFinder: Doublet Detection in Single-Cell RNA Sequencing Data Using Artificial Nearest Neighbors. Cell Syst *8*, 329-337 e324.
Moreno-Jimenez, E.P., Terreros-Roncal, J., Flor-Garcia, M., Rabano, A., and Llorens-Martin, M. (2021). Evidences for Adult Hippocampal Neurogenesis in Humans. J Neurosci *41*, 2541-2553.
Motori, E., Atanassov, I., Kochan, S.M.V., Folz-Donahue, K., Sakthivelu, V., Giavalisco, P., Toni, N., Puyal, J., and Larsson, N.G. (2020). Neuronal metabolic rewiring promotes resilience to neurodegeneration caused by mitochondrial dysfunction. Sci Adv *6*, eaba8271.
Murata, K., Kinoshita, T., Ishikawa, T., Kuroda, K., Hoshi, M., and Fukazawa, Y. (2020). Region- and neuronal-subtype-specific expression of Na,K-ATPase alpha and beta subunit isoforms in the mouse brain. J Comp Neurol *528*, 2654-2678.
Negash, S., Wilson, R.S., Leurgans, S.E., Wolk, D.A., Schneider, J.A., Buchman, A.S., Bennett, D.A., and Arnold, S.E. (2013). Resilient brain aging: characterization of discordance between Alzheimer's disease pathology and cognition. Curr Alzheimer Res *10*, 844-851.
Neuner, S.M., Garfinkel, B.P., Wilmott, L.A., Ignatowska-Jankowska, B.M., Citri, A., Orly, J., Lu, L., Overall, R.W., Mulligan, M.K., Kempermann, G.*, et al.* (2016). Systems genetics identifies Hp1bp3 as a novel modulator of cognitive aging. Neurobiol Aging *46*, 58-67.
Neuner, S.M., Heuer, S.E., Huentelman, M.J., O'Connell, K.M.S., and Kaczorowski, C.C. (2019a). Harnessing Genetic Complexity to Enhance Translatability of Alzheimer's Disease Mouse Models: A Path toward Precision Medicine. Neuron *101*, 399-411 e395.
Neuner, S.M., Heuer, S.E., Zhang, J.G., Philip, V.M., and Kaczorowski, C.C. (2019b). Identification of Pre-symptomatic Gene Signatures That Predict Resilience to Cognitive Decline in the Genetically Diverse AD-BXD Model. Front Genet *10*, 35.

Neuner, S.M., Telpoukhovskaia, M., Menon, V., O'Connell, K.M.S., Hohman, T.J., and Kaczorowski, C.C. (2022). Translational approaches to understanding resilience to Alzheimer's disease. Trends in Neurosciences.
Neuner, S.M., Wilmott, L., DeBoth, M., Shapaker, T., Ingels, J., Lu, L., Williams, R., Kempermann, G., Huentelman, M., and Kaczorowski, C.C. (2015a). Multi-scale study of normal aging predicts novel late-onset Alzheimer's disease risk variants. BMC Bioinformatics *16*.
Neuner, S.M., Wilmott, L.A., Hope, K.A., Hoffmann, B., Chong, J.A., Abramowitz, J., Birnbaumer, L., O'Connell, K.M., Tryba, A.K., Greene, A.S.*, et al.* (2015b). TRPC3 channels critically regulate hippocampal excitability and contextual fear memory. Behav Brain Res *281*, 69-77.
Oakley, H., Cole, S.L., Logan, S., Maus, E., Shao, P., Craft, J., Guillozet-Bongaarts, A., Ohno, M., Disterhoft, J., Van Eldik, L.*, et al.* (2006). Intraneuronal beta-amyloid aggregates, neurodegeneration, and neuron loss in transgenic mice with five familial Alzheimer's disease mutations: potential factors in amyloid plaque formation. J Neurosci *26*, 10129-10140.
Oblak, A.L., Forner, S., Territo, P.R., Sasner, M., Carter, G.W., Howell, G.R., Sukoff-Rizzo, S.J., Logsdon, B.A., Mangravite, L.M., Mortazavi, A.*, et al.* (2020). Model organism development and evaluation for late-onset Alzheimer's disease: MODEL-AD. Alzheimers Dement (N Y) *6*, e12110.
Ou, Y.N., Yang, Y.X., Deng, Y.T., Zhang, C., Hu, H., Wu, B.S., Liu, Y., Wang, Y.J., Zhu, Y., Suckling, J.*, et al.* (2021). Identification of novel drug targets for Alzheimer's disease by integrating genetics and proteomes from brain and blood. Mol Psychiatry *26*, 6065-6073.
Peirce, J.L., Lu, L., Gu, J., Silver, L.M., and Williams, R.W. (2004). A new set of BXD recombinant inbred lines from advanced intercross populations in mice. BMC Genet *5*, 7.
Perez-Nievas, B.G., Stein, T.D., Tai, H.C., Dols-Icardo, O., Scotton, T.C., Barroeta-Espar, I., Fernandez-Carballo, L., de Munain, E.L., Perez, J., Marquie, M.*, et al.* (2013). Dissecting phenotypic traits linked to human resilience to Alzheimer's pathology. Brain *136*, 2510-2526.
R Core Team (2021). R: A language and environment for statistical computing. (Vienna, Austria: R Foundation for Statistical Computing).
Saul, M.C., Philip, V.M., Reinholdt, L.G., Center for Systems Neurogenetics of, A., and Chesler, E.J. (2019). High-Diversity Mouse Populations for Complex Traits. Trends Genet *35*, 501-514.
Simko, T.W.a.V. (2021). R package "corrplot": Visualization of a Correlation Matrix.
Simo, S., Jossin, Y., and Cooper, J.A. (2010). Cullin 5 regulates cortical layering by modulating the speed and duration of Dab1-dependent neuronal migration. J Neurosci *30*, 5668-5676.
Sorrells, S.F., Paredes, M.F., Zhang, Z., Kang, G., Pastor-Alonso, O., Biagiotti, S., Page, C.E., Sandoval, K., Knox, A., Connolly, A.*, et al.* (2021). Positive Controls in Adults and Children Support That Very Few, If Any, New Neurons Are Born in the Adult Human Hippocampus. J Neurosci *41*, 2554-2565.
Srinivasan, K., Friedman, B.A., Etxeberria, A., Huntley, M.A., van der Brug, M.P., Foreman, O., Paw, J.S., Modrusan, Z., Beach, T.G., Serrano, G.E.*, et al.* (2020). Alzheimer's Patient Microglia Exhibit Enhanced Aging and Unique Transcriptional Activation. Cell Rep *31*, 107843.
Stuart, T., Butler, A., Hoffman, P., Hafemeister, C., Papalexi, E., Mauck, W.M., 3rd, Hao, Y., Stoeckius, M., Smibert, P., and Satija, R. (2019). Comprehensive Integration of Single-Cell Data. Cell *177*, 1888-1902 e1821.
Taylor, B.A., Wnek, C., Kotlus, B.S., Roemer, N., MacTaggart, T., and Phillips, S.J. (1999). Genotyping new BXD recombinant inbred mouse strains and comparison of BXD and consensus maps. Mamm Genome *10*, 335-348.
Terreros-Roncal, J., Moreno-Jimenez, E.P., Flor-Garcia, M., Rodriguez-Moreno, C.B., Trinchero, M.F., Cafini, F., Rabano, A., and Llorens-Martin, M. (2021). Impact of neurodegenerative diseases on human adult hippocampal neurogenesis. Science *374*, 1106-1113.
Tobin, M.K., Musaraca, K., Disouky, A., Shetti, A., Bheri, A., Honer, W.G., Kim, N., Dawe, R.J., Bennett, D.A., Arfanakis, K.*, et al.* (2019). Human Hippocampal Neurogenesis Persists in Aged Adults and Alzheimer's Disease Patients. Cell Stem Cell *24*, 974-982 e973.
Wan, Y.W., Al-Ouran, R., Mangleburg, C.G., Perumal, T.M., Lee, T.V., Allison, K., Swarup, V., Funk, C.C., Gaiteri, C., Allen, M.*, et al.* (2020). Meta-Analysis of the Alzheimer's Disease Human Brain Transcriptome and Functional Dissection in Mouse Models. Cell Rep *32*, 107908.
Wang, Q., Ding, S.L., Li, Y., Royall, J., Feng, D., Lesnar, P., Graddis, N., Naeemi, M., Facer, B., Ho, A.*, et al.* (2020). The Allen Mouse Brain Common Coordinate Framework: A 3D Reference Atlas. Cell *181*, 936-953 e920.

Wang, X., Xia, W., Li, K., Zhang, Y., Ge, W., and Ma, C. (2019). Rapamycin regulates cholesterol biosynthesis and cytoplasmic ribosomal proteins in hippocampus and temporal lobe of APP/PS1 mouse. J Neurol Sci *399*, 125-139.
Weisberg, J.F.a.S. (2019). An {R} Companion to Applied Regression, Third edn (Thousand Oaks, CA: Sage).
Welch, J., Gao, C., Liu, J., Sodicoff, J., Kozareva, V., and Macosko, E. (2021). rliger: Linked Inference of Genomic Experimental Relationships.
Welch, J.D., Kozareva, V., Ferreira, A., Vanderburg, C., Martin, C., and Macosko, E.Z. (2019). Single-Cell Multi-omic Integration Compares and Contrasts Features of Brain Cell Identity. Cell *177*, 1873-1887 e1817.
West, M.J., Kawas, C.H., Stewart, W.F., Rudow, G.L., and Troncoso, J.C. (2004). Hippocampal neurons in pre-clinical Alzheimer's disease. Neurobiol Aging *25*, 1205-1212.
White, C.C., Yang, H.S., Yu, L., Chibnik, L.B., Dawe, R.J., Yang, J., Klein, H.U., Felsky, D., Ramos-Miguel, A., Arfanakis, K.*, et al.* (2017). Identification of genes associated with dissociation of cognitive performance and neuropathological burden: Multistep analysis of genetic, epigenetic, and transcriptional data. PLoS Med *14*, e1002287.
Wilson, R.S., Boyle, P.A., Yu, L., Barnes, L.L., Sytsma, J., Buchman, A.S., Bennett, D.A., and Schneider, J.A. (2015). Temporal course and pathologic basis of unawareness of memory loss in dementia. Neurology *85*, 984-991.
Wu, T., Hu, E., Xu, S., Chen, M., Guo, P., Dai, Z., Feng, T., Zhou, L., Tang, W., Zhan, L.*, et al.* (2021). clusterProfiler 4.0: A universal enrichment tool for interpreting omics data. Innovation (N Y) *2*, 100141.
Xu, R., Li, X., Boreland, A.J., Posyton, A., Kwan, K., Hart, R.P., and Jiang, P. (2020). Human iPSC-derived mature microglia retain their identity and functionally integrate in the chimeric mouse brain. Nat Commun *11*, 1577.
Yang, H.S., White, C.C., Klein, H.U., Yu, L., Gaiteri, C., Ma, Y., Felsky, D., Mostafavi, S., Petyuk, V.A., Sperling, R.A.*, et al.* (2020). Genetics of Gene Expression in the Aging Human Brain Reveal TDP-43 Proteinopathy Pathophysiology. Neuron *107*, 496-508 e496.
Yates, S.C., Groeneboom, N.E., Coello, C., Lichtenthaler, S.F., Kuhn, P.H., Demuth, H.U., Hartlage-Rubsamen, M., Rossner, S., Leergaard, T., Kreshuk, A.*, et al.* (2019). QUINT: Workflow for Quantification and Spatial Analysis of Features in Histological Images From Rodent Brain. Front Neuroinform *13*, 75.
Yu, L., Tasaki, S., Schneider, J.A., Arfanakis, K., Duong, D.M., Wingo, A.P., Wingo, T.S., Kearns, N., Thatcher, G.R.J., Seyfried, N.T.*, et al.* (2020). Cortical Proteins Associated With Cognitive Resilience in Community-Dwelling Older Persons. JAMA Psychiatry *77*, 1172-1180.
Zheng, G.X., Terry, J.M., Belgrader, P., Ryvkin, P., Bent, Z.W., Wilson, R., Ziraldo, S.B., Wheeler, T.D., McDermott, G.P., Zhu, J.*, et al.* (2017). Massively parallel digital transcriptional profiling of single cells. Nat Commun *8*, 14049.
Zhong, S., Zhang, S., Fan, X., Wu, Q., Yan, L., Dong, J., Zhang, H., Li, L., Sun, L., Pan, N.*, et al.* (2018). A single-cell RNA-seq survey of the developmental landscape of the human prefrontal cortex. Nature *555*, 524-528.

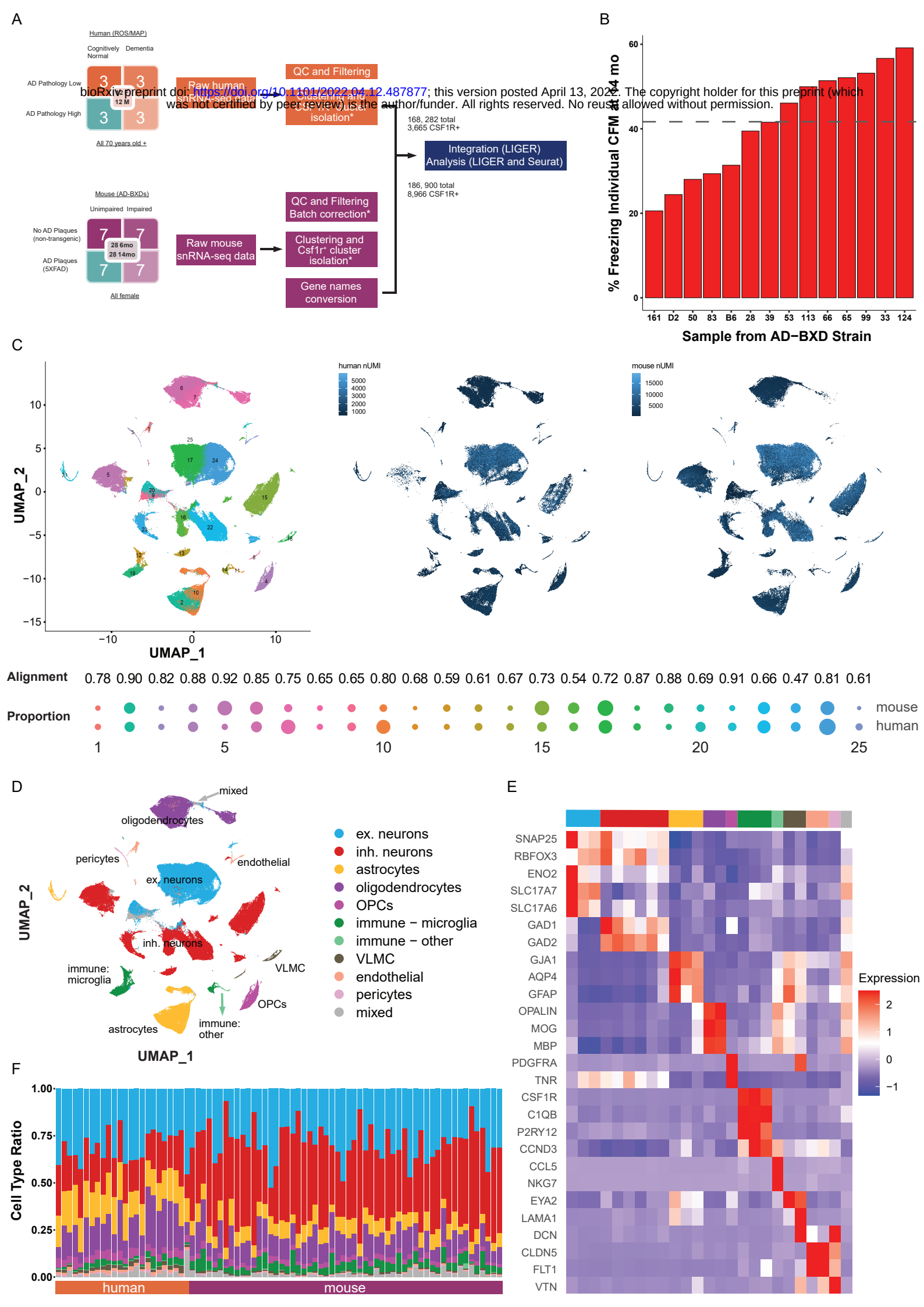

Fig. 1. Integration of human and mouse snRNA-seq PFC data resulted in a shared data space with no compositional differences between resilient and susceptible individuals. **A.** Cohort demographics and analysis workflow for cross-species data integration; **B.** Plot of CFM values to define resilient and susceptible status for the 14 mo mice with 5XFAD transgene; **C.** Integrated human and mouse data set: UMAP visualization of the integrated data set with cluster numbers, and separate UMAP of the data for human (left) and mouse (right); alignment per cluster and cluster proportion by species below; **D.** MetaNeighbor analysis and differential gene expression led to classification of each cluster as a cell type. Heatmap with cell-type specific marker genes demonstrate cell-type assignments. Heatmap was produced using average expression for each cluster, by default, with scaled data and maximum display value set at 2.5; **E.** UMAP for the integrated data set with cluster identity; **F.** Proportions of cell types in each sample.

A

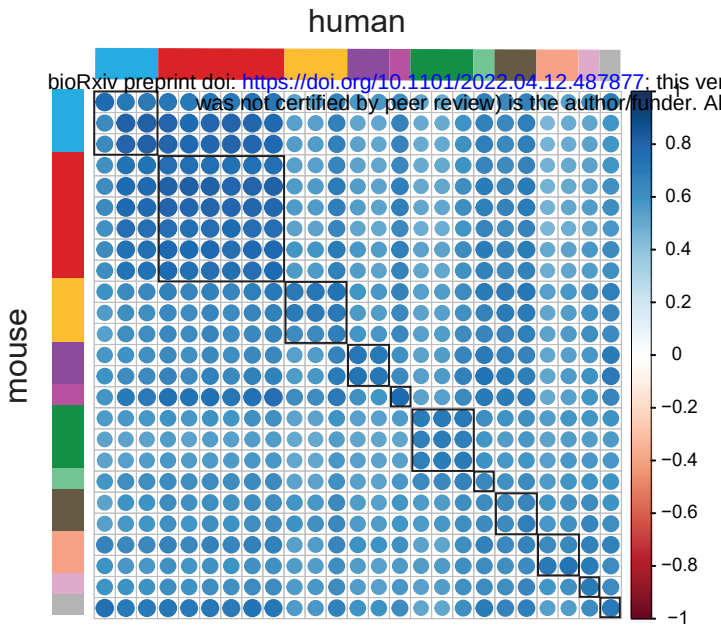

B

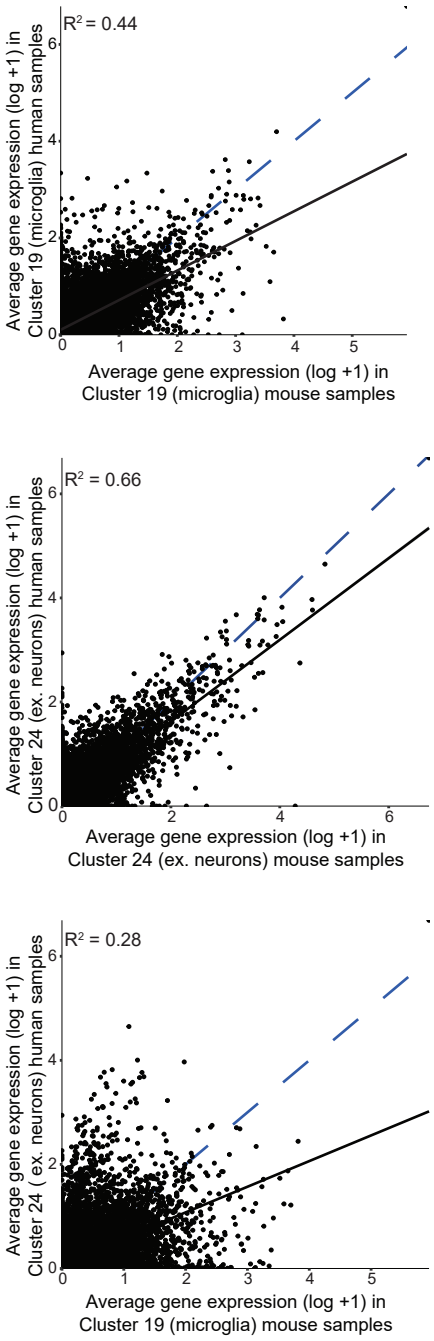

C

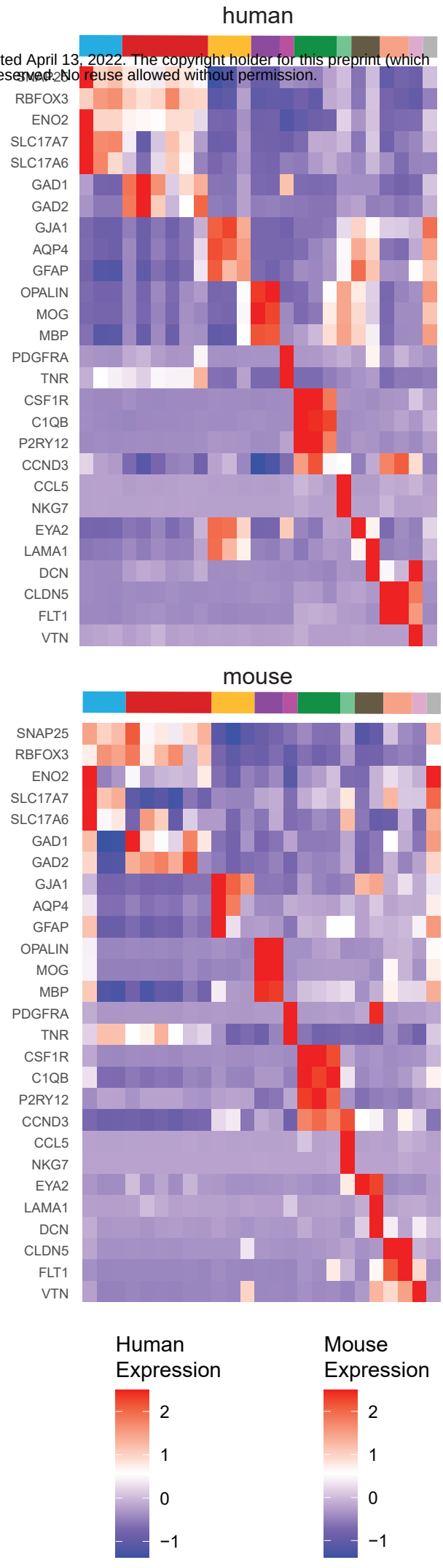

Fig. 2. Correlation analysis of genes per cluster and separate UMAPs for each species. A. Correlation plot of genes in each cluster across species; **B.** Example correlations showing each gene for a microglia cluster in human and mouse, for an ex. neuronal cluster for human and mouse, and for a microglia mouse cluster vs a human neuronal cluster with lower correlation value, with dashed blue line representing perfect concordance (slope of 1) and the solid black line the fit of the data used to calculate R^2 value; **C.** Individual heatmaps for human and mouse data within the integrated clusters demonstrating a shared class identity in all but one cluster (right most cluster, #9).

A

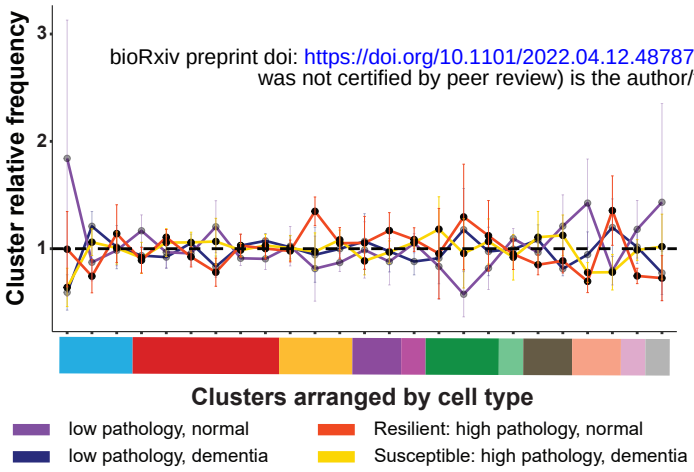

B

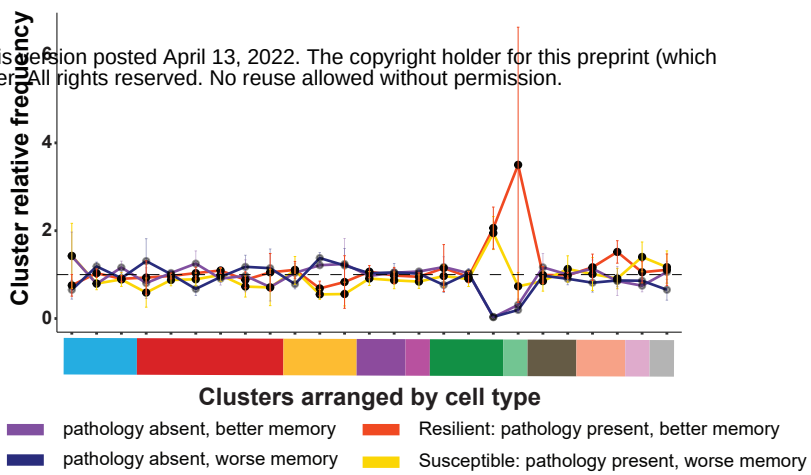

C

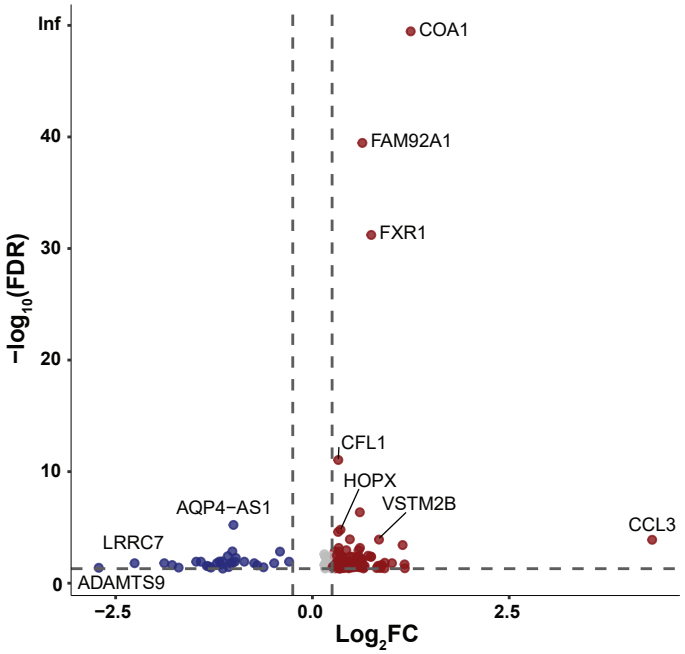

D

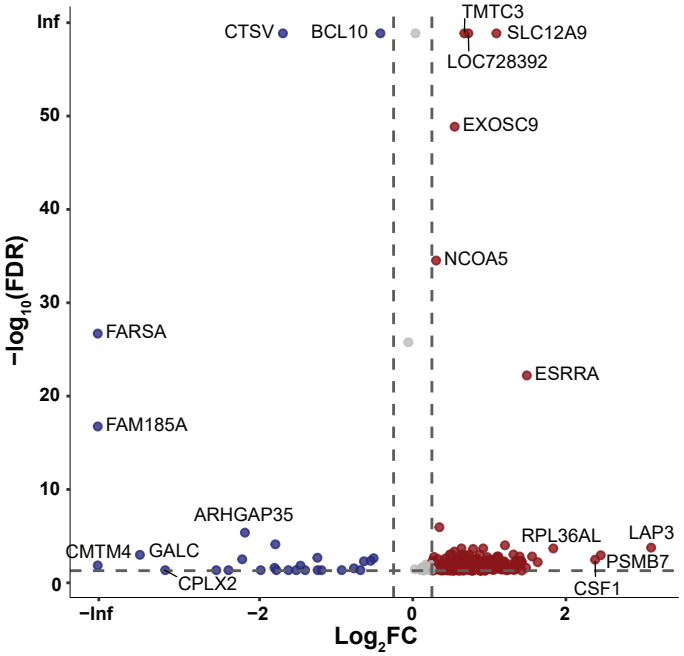

E

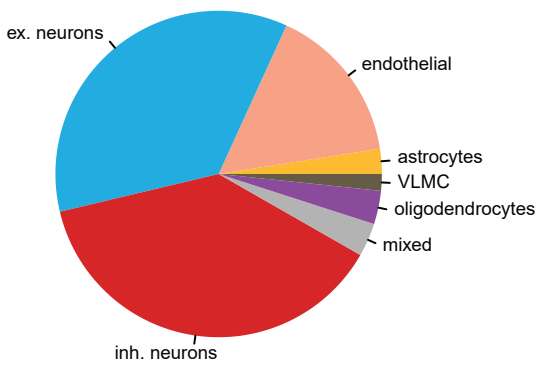

F

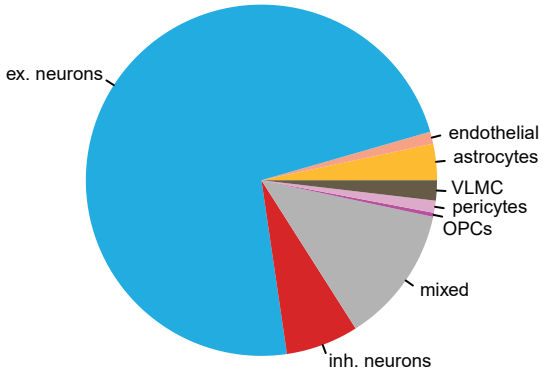

Fig. 3. Resilient transcriptional signatures identified in excitatory cluster shared cross-species. A and **B**. Composition of all the sample groups in each cluster for human subjects with pathology (**A**) and 14 mo mice with 5XFAD transgene (**B**), with resilient and susceptible groups with more saturated color. No statistical differences were found between the resilient and susceptible groups in each cluster (t-test with Benjamini-Hochberg multiple comparison correction); **C** and **D.** Volcano plots with significantly differentially expressed genes between resilient and susceptible individuals (each dot), for human (**C**) and 14 mo mouse subjects (**D**). Blue color indicates downregulation in resilient individuals ($log_2FC \leq - 0.25$) and red color indicates upregulation in resilient individuals ($log_2FC \geq 0.25$); **E** and **F**. Pie charts demonstrating cell type identity of clusters for differentially expressed genes from **C** and **D**. In both in human (**E**) and mouse (**F**), most genes are from neuronal clusters.

A

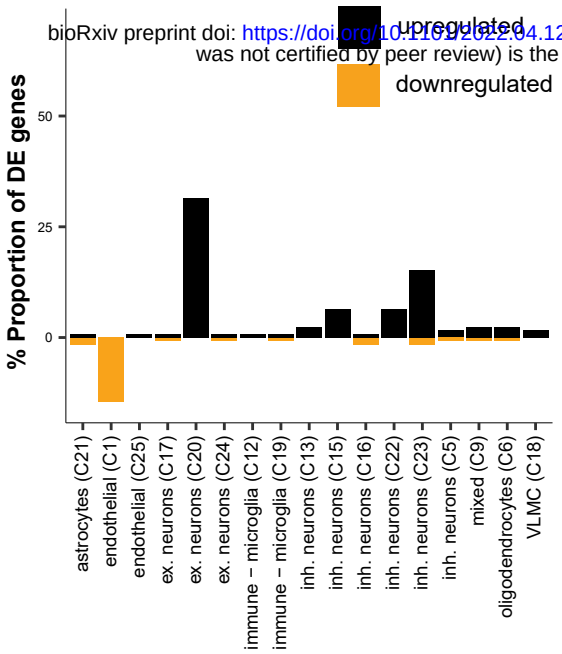

B

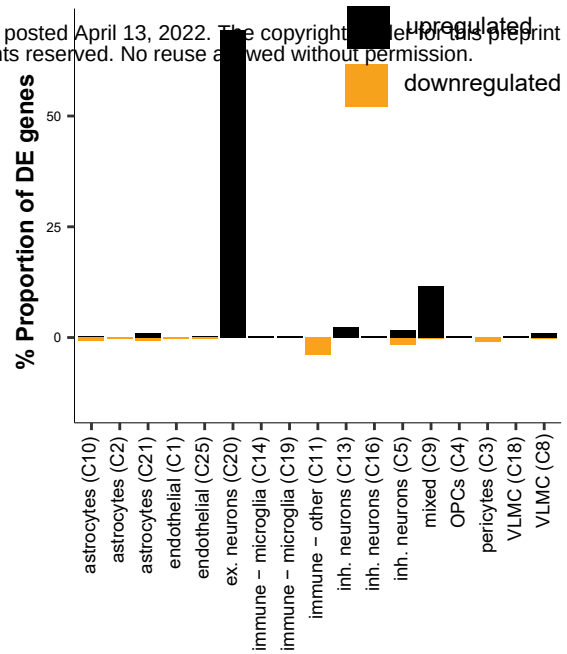

C

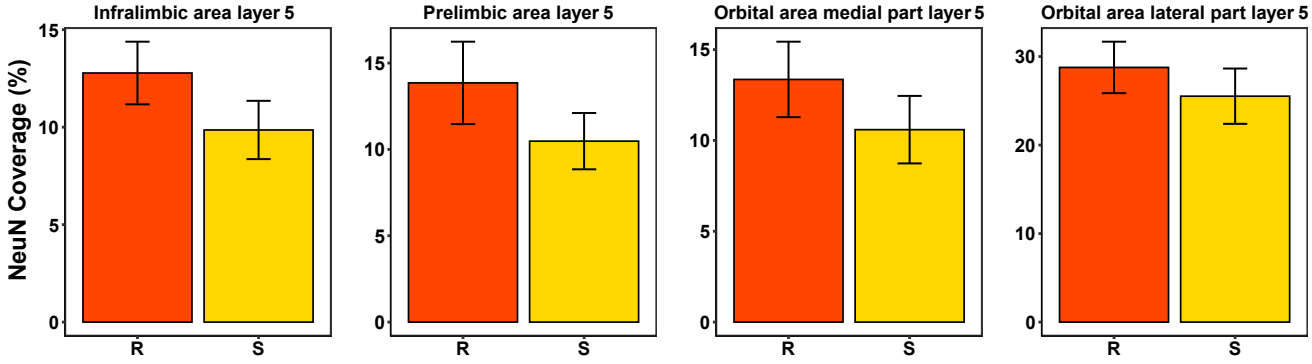

D

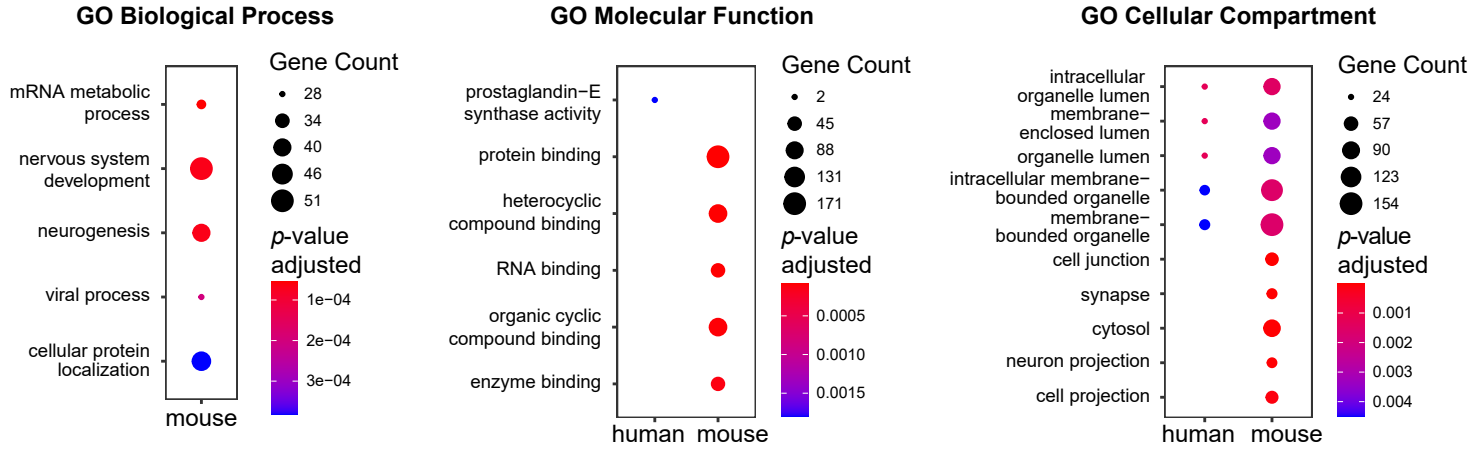

Fig. 4. Resilience gene network characterization. A and **B.** Proportional significantly differentially expressed (adjusted p-value ≤ 0.05) upregulated and downregulated genes in the human subjects with pathology (**A**) and the 14 mo mice with 5XFAD transgene (**B**) showing most genes were upregulated ($log_2FC \geq 0.25$) and are particularly enriched in cluster 20; **C.** Bar graphs of NeuN coverage in multiple layer 5 regions (orbital area, prelimbic area, and infralimbic area) demonstrate no difference between resilient and susceptible strains. Values with 0% coverage due to absence of area in sections were removed; **D.** GO enrichment analyses for human and mouse gene lists identified pathways in the mouse data set (5 top pathways included for each species, adjusted p-value threshold of 0.05).

A

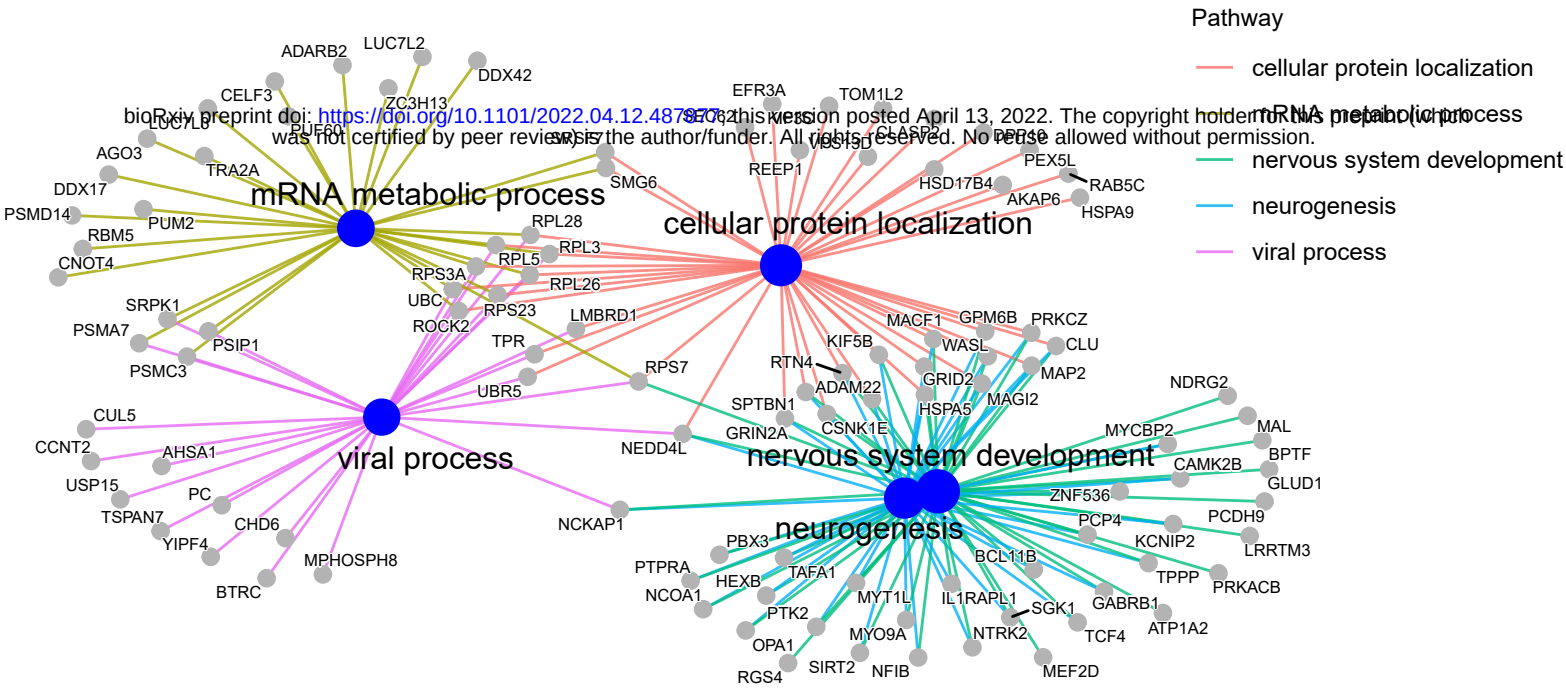

Fig. 5. Mouse resilience gene characterization. A. Gene concept network demonstrating gene linkages among the top 5 GO:BP terms demonstrating overlap and differentiation of gene function: cellular protein localization (43 genes), mRNA metabolic process (29 genes), nervous system development (51 genes), neurogenesis (40 genes), viral process (28 genes).

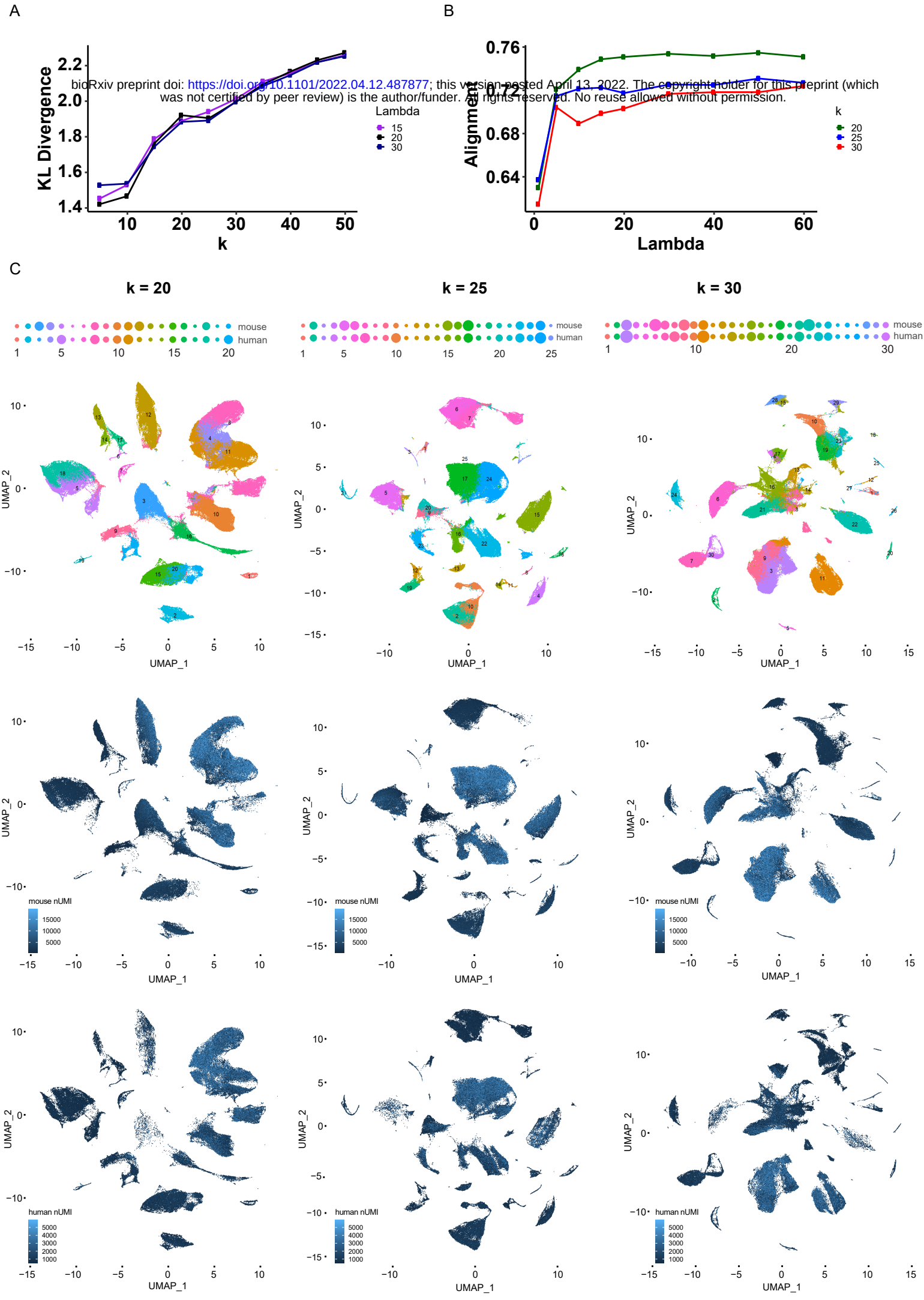

Fig. S1. Parameter optimization for LIGER integration. A. KL divergence plot varying lambda (15, 20, 30) and **B.** alignment plot varying k (20, 25, 30) for parameter selection for LIGER integration; **C.** Integrated human and mouse data set with lambda = 30, varying k (20 (left), 25 (middle), 30 (right)): cluster proportion by species, UMAP visualization of the integrated data set with cluster numbers, and separate UMAP of the data for mouse (top) and human (bottom).

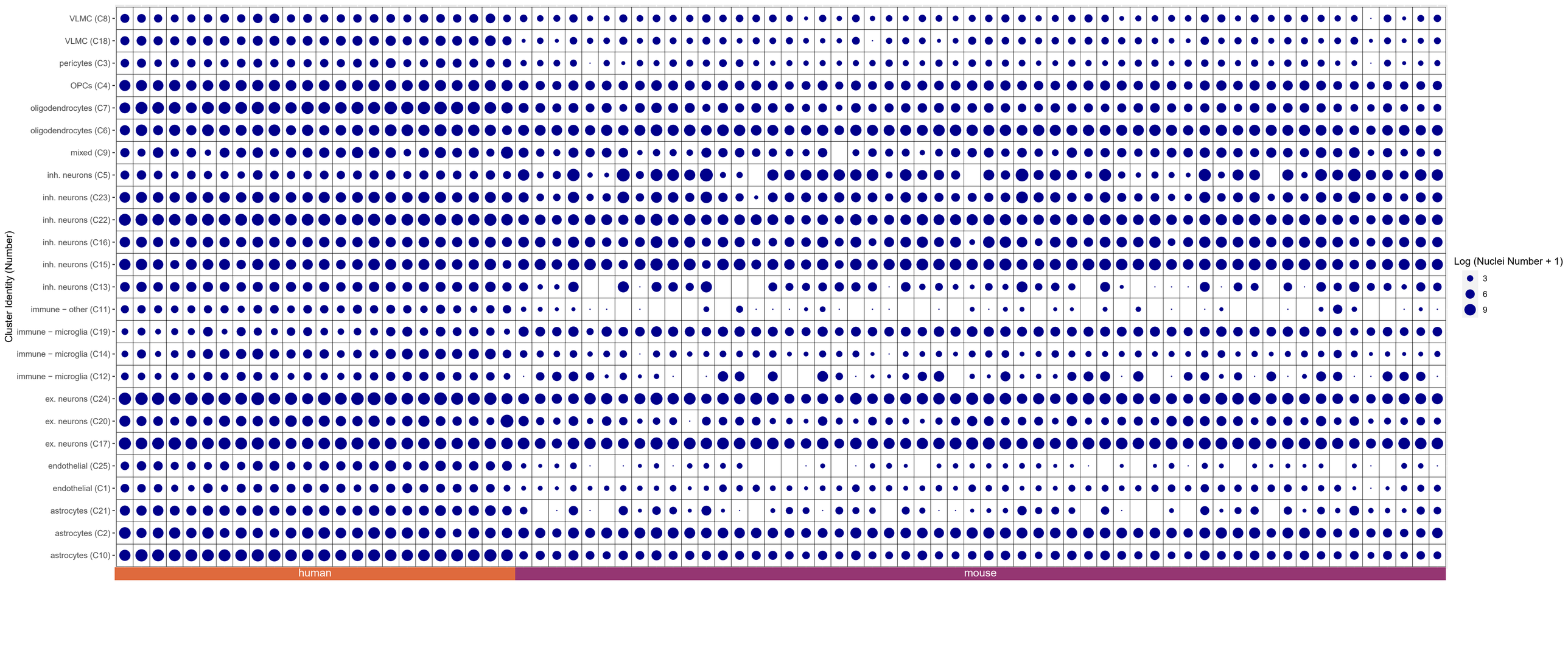
VLMC (C8)
VLMC (C18)
pericytes (C3)
OPCs (C4)
oligodendrocytes (C7)
oligodendrocytes (C6)
mixed (C9)
inh. neurons (C5)
inh. neurons (C23)
inh. neurons (C22)
inh. neurons (C16)
inh. neurons (C15)
inh. neurons (C13)
immune − other (C11)
immune − microglia (C19)
immune − microglia (C14)
immune − microglia (C12)
ex. neurons (C24)
ex. neurons (C20)
ex. neurons (C17)
endothelial (C25)
endothelial (C1)
astrocytes (C21)
astrocytes (C2)
astrocytes (C10)
Cluster Identity (Number)
human
mouse
Log (Nuclei Number + 1)
3
6
9

Fig. S2. **Log of nuclei numbers in each cluster for each sample.**

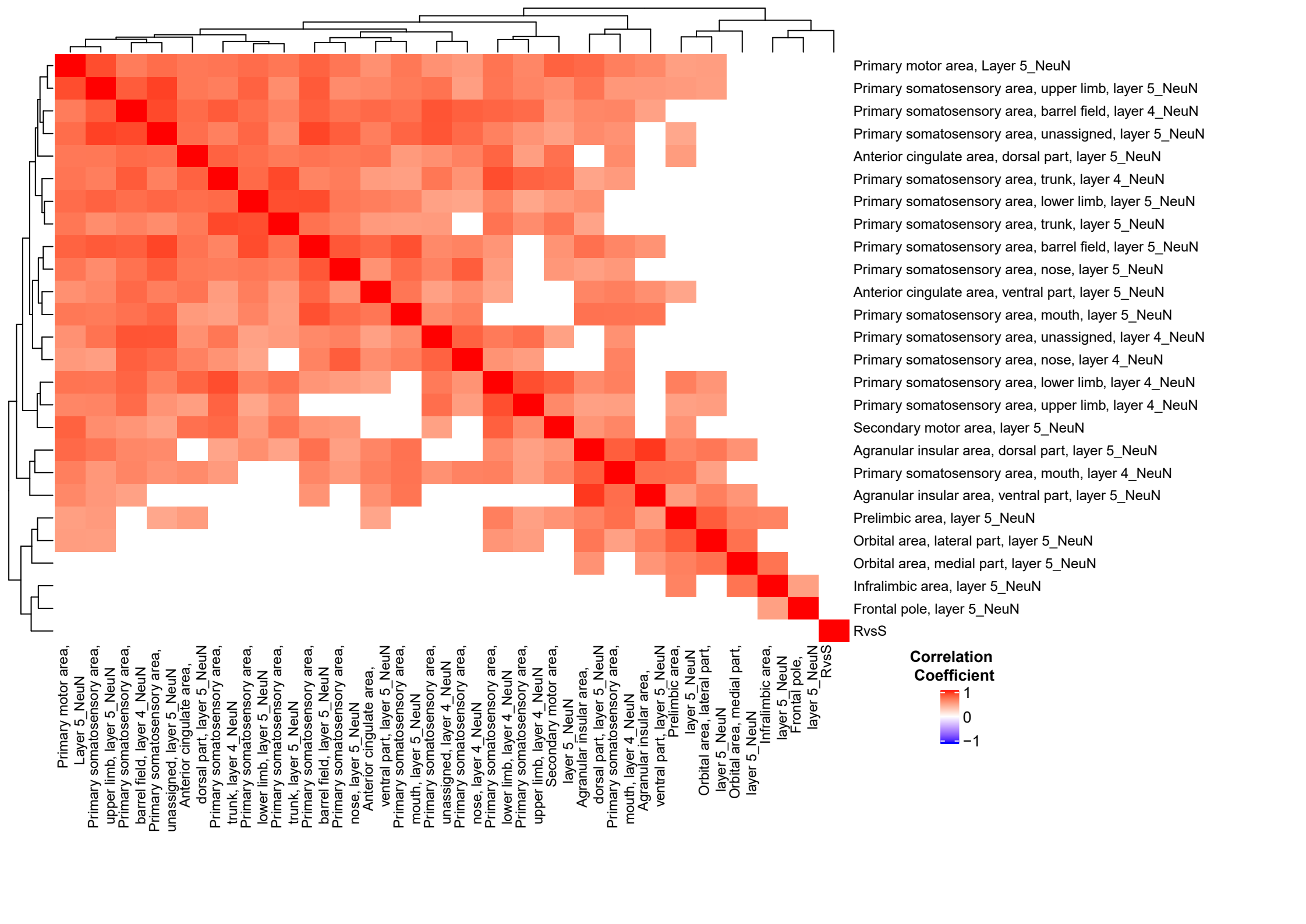
Primary motor area, Layer 5_NeuN
Primary somatosensory area, upper limb, layer 5_NeuN
Primary somatosensory area, barrel field, layer 4_NeuN
Primary somatosensory area, unassigned, layer 5_NeuN
Anterior cingulate area, dorsal part, layer 5_NeuN
Primary somatosensory area, trunk, layer 4_NeuN
Primary somatosensory area, lower limb, layer 5_NeuN
Primary somatosensory area, trunk, layer 5_NeuN
Primary somatosensory area, barrel field, layer 5_NeuN
Primary somatosensory area, nose, layer 5_NeuN
Anterior cingulate area, ventral part, layer 5_NeuN
Primary somatosensory area, mouth, layer 5_NeuN
Primary somatosensory area, unassigned, layer 4_NeuN
Primary somatosensory area, nose, layer 4_NeuN
Primary somatosensory area, lower limb, layer 4_NeuN
Primary somatosensory area, upper limb, layer 4_NeuN
Secondary motor area, layer 5_NeuN
Agranular insular area, dorsal part, layer 5_NeuN
Primary somatosensory area, mouth, layer 4_NeuN
Agranular insular area, ventral part, layer 5_NeuN
Prelimbic area, layer 5_NeuN
Orbital area, lateral part, layer 5_NeuN
Orbital area, medial part, layer 5_NeuN
Infralimbic area, layer 5_NeuN
Frontal pole, layer 5_NeuN
RvsS
Correlation Coefficient
1
0
−1

Fig. S3. Correlation plot for NeuN coverage among different layer 4 and 5 regions and cognitive status in AD-BXD strains.

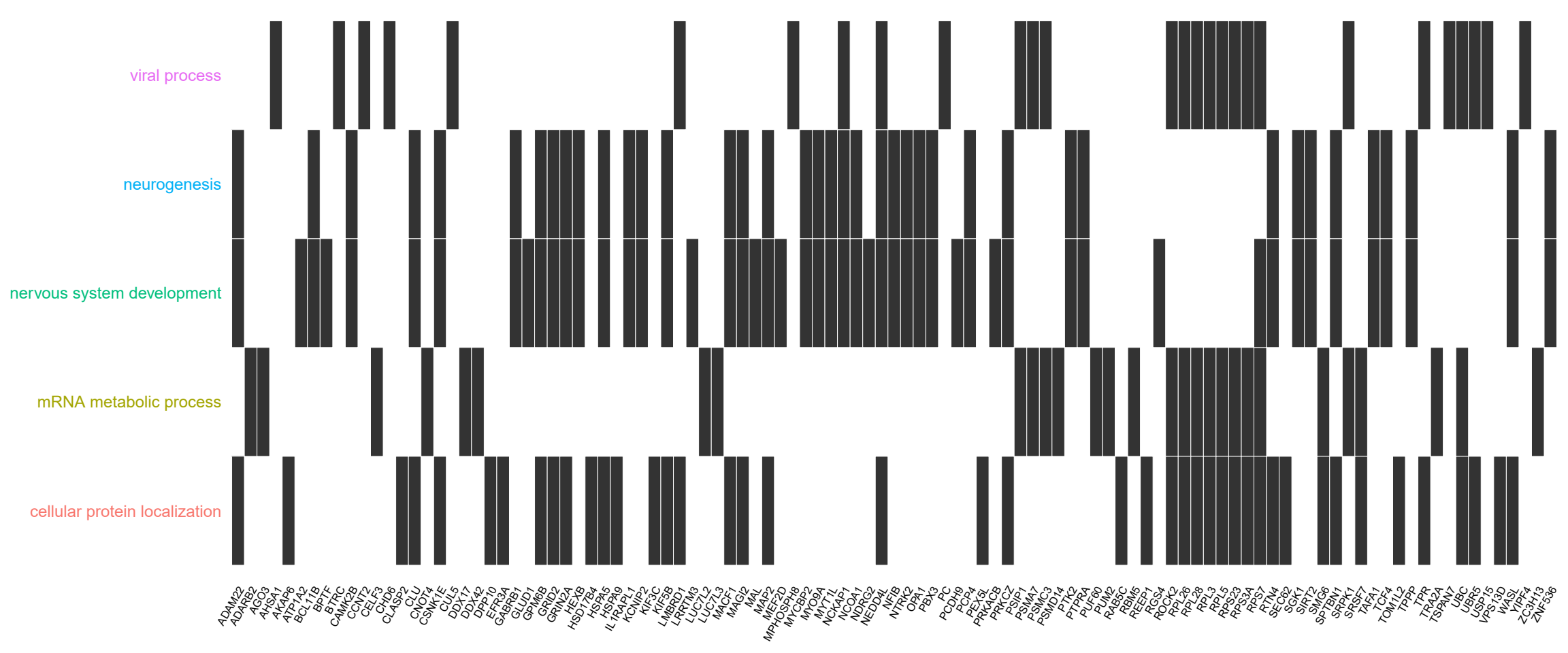
viral process
neurogenesis
nervous system development
mRNA metabolic process
cellular protein localization
ADAM22
ADARB2
AGO3
AHSA1
AKAP6
ATP1A2
BCL11B
BPTF
BTRC
CAMK2B
CCNT2
CELF3
CHD6
CLASP2
CLU
CNOT4
CSNK1E
CUL5
DDX17
DDX42
DPP10
EFR3A
GABRB1
GLUD1
GPM6B
GRID2
GRIN2A
HEXB
HSD17B4
HSPA5
HSPA9
IL1RAPL1
KCNIP2
KIF3C
KIF5B
LMBRD1
LRRTM3
LUC7L2
LUC7L3
MACF1
MAGI2
MAL
MAP2
MEF2D
MPHOSPH8
MYCBP2
MYO9A
MYT1L
NCKAP1
NCOA1
NDRG2
NEDD4L
NFIB
NTRK2
OPA1
PBX3
PC
PCDH9
PCP4
PEX5L
PRKACB
PRKCZ
PSIP1
PSMA7
PSMC3
PSMD14
PTK2
PTPRA
PUF60
PUM2
RAB5C
RBM5
REEP1
RGS4
ROCK2
RPL26
RPL28
RPL3
RPL5
RPS23
RPS3A
RPS7
RTN4
SEC62
SGK1
SIRT2
SMG6
SPTBN1
SRRK1
SRSF7
TAFA1
TCF4
TOM1L2
TPPP
TPR
TRA2A
TSPAN7
UBC
UBR5
USP15
VPS13D
WASL
YIPF4
ZC3H13
ZNF536

Fig. S4. Companion plot for Fig. 5 for each gene membership in top 5 GO:BP pathways.

A

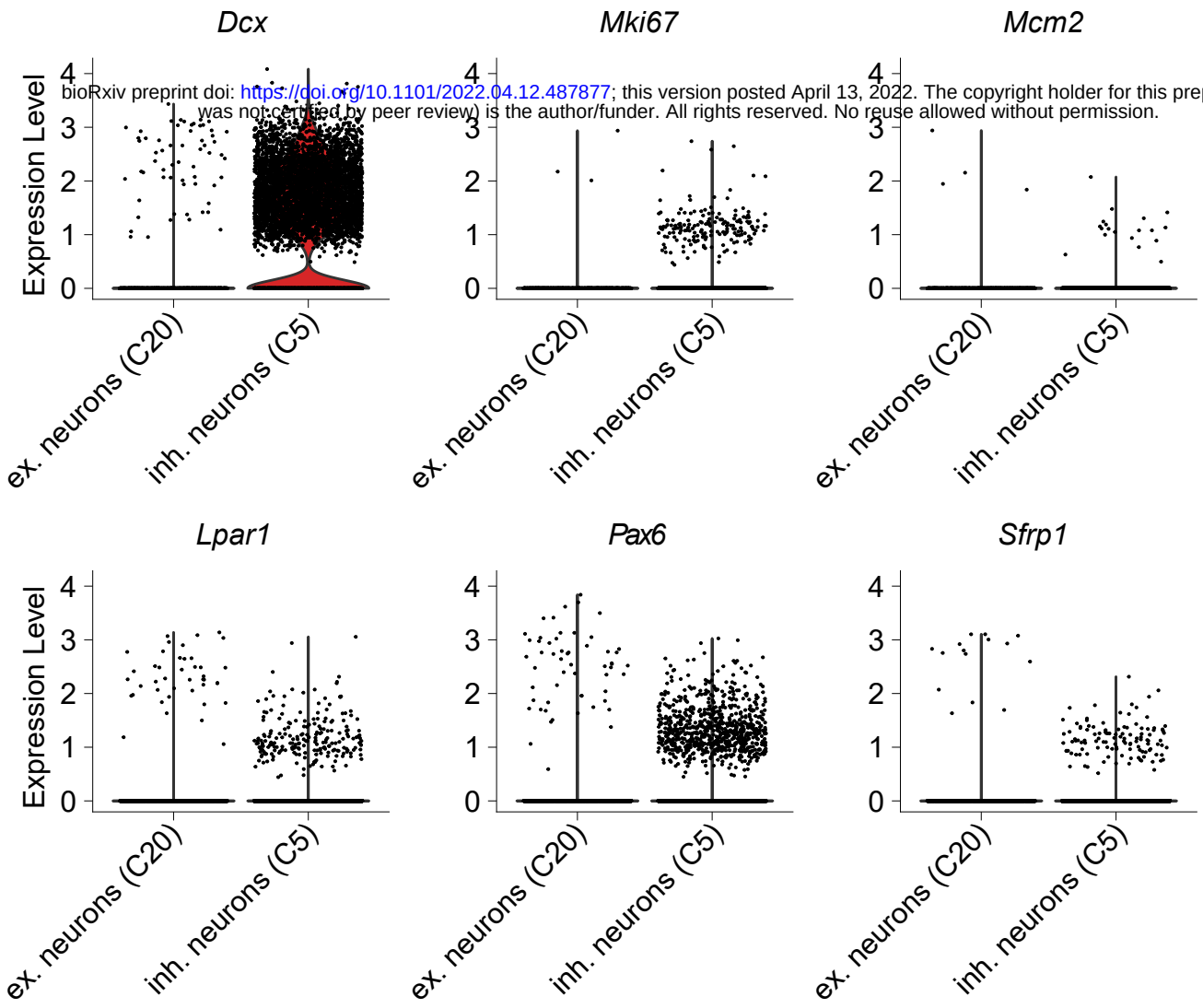

Fig. S5. Expression level for neurogenesis-related genes in excitatory neuronal cluster 20 and inhibitory neuronal cluster 5.

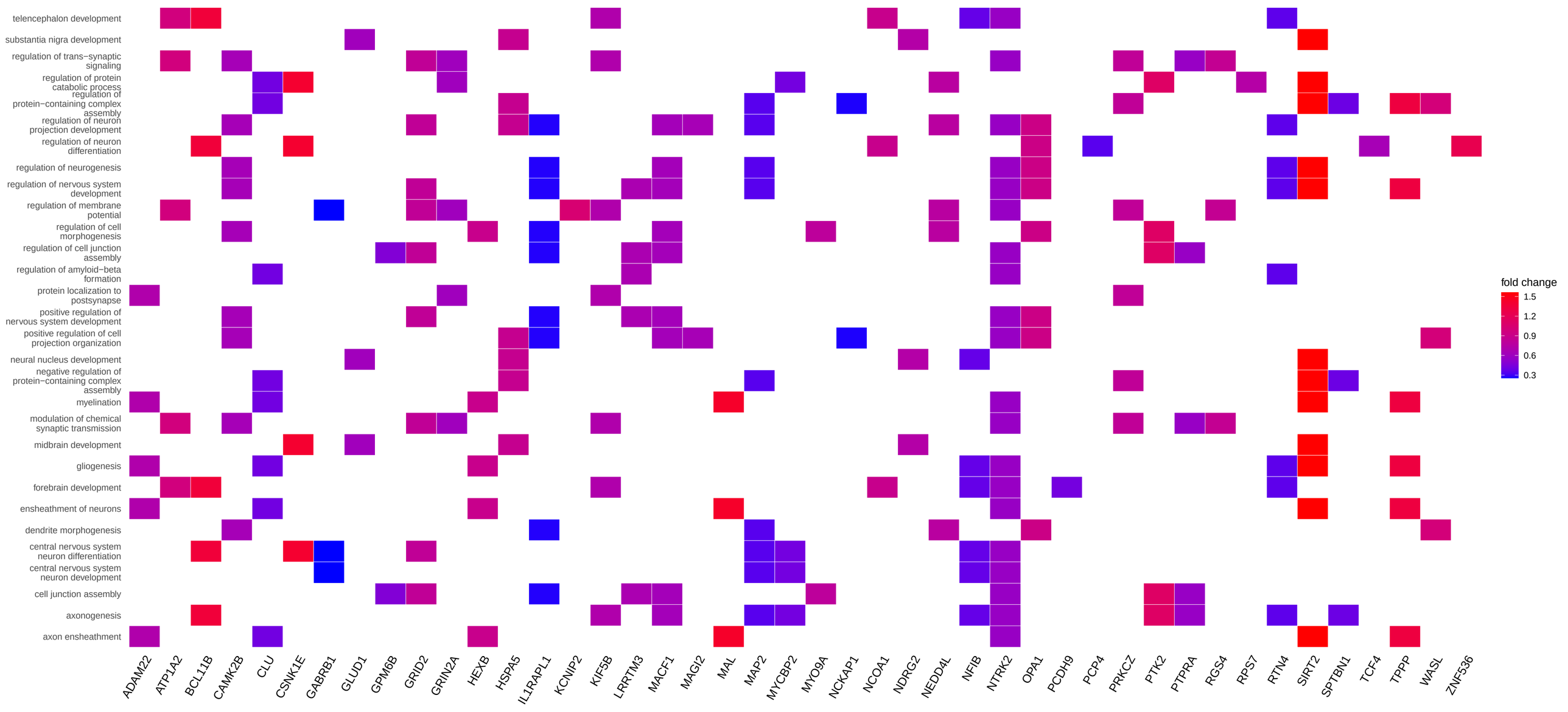
telencephalon development
substantia nigra development
regulation of trans−synaptic signaling
regulation of protein catabolic process
regulation of protein−containing complex assembly
regulation of neuron projection development
regulation of neuron differentiation
regulation of neurogenesis
regulation of nervous system development
regulation of membrane potential
regulation of cell morphogenesis
regulation of cell junction assembly
regulation of amyloid−beta formation
protein localization to postsynapse
positive regulation of nervous system development
positive regulation of cell projection organization
neural nucleus development
negative regulation of protein−containing complex assembly
myelination
modulation of chemical synaptic transmission
midbrain development
gliogenesis
forebrain development
ensheathment of neurons
dendrite morphogenesis
central nervous system neuron differentiation
central nervous system neuron development
cell junction assembly
axonogenesis
axon ensheathment
ADAM22
ATP1A2
BCL11B
CAMK2B
CLU
CSNK1E
GABRB1
GLUD1
GPM6B
GRID2
GRIN2A
HEXB
HSPA5
IL1RAPL1
KCNIP2
KIF5B
LRRTM3
MACF1
MAGI2
MAL
MAP2
MYCBP2
MYO9A
NCKAP1
NCOA1
NDRG2
NEDD4L
NFIB
NTRK2
OPA1
PCDH9
PCP4
PRKCZ
PTK2
PTPRA
RGS4
RPS7
RTN4
SIRT2
SPTBN1
TCF4
TPPP
WASL
ZNF536
fold change
1.5
1.2
0.9
0.6
0.3

Fig. S6. Gene membership in top 30 GO:BP pathways among nervous development genes from Figs. 5 and S4.

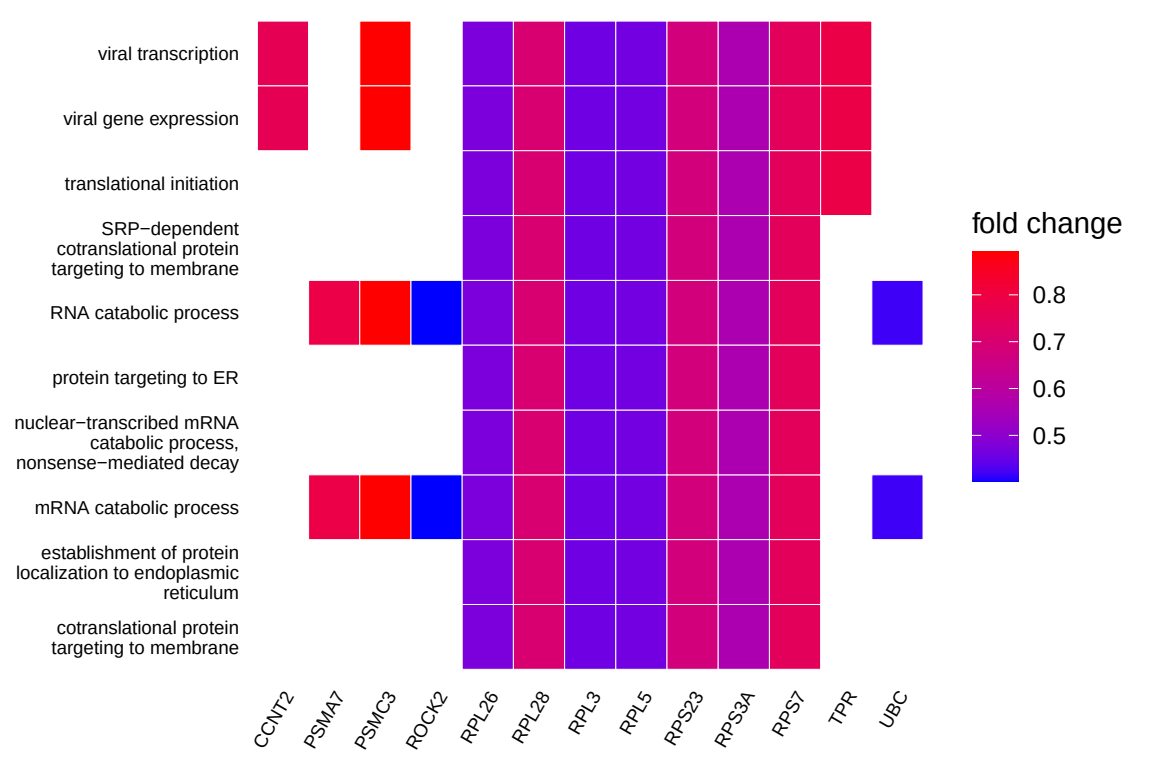
viral transcription
viral gene expression
translational initiation
SRP−dependent cotranslational protein targeting to membrane
RNA catabolic process
protein targeting to ER
nuclear−transcribed mRNA catabolic process, nonsense−mediated decay
mRNA catabolic process
establishment of protein localization to endoplasmic reticulum
cotranslational protein targeting to membrane
CCNT2
PSMA7
PSMC3
ROCK2
RPL26
RPL28
RPL3
RPL5
RPS23
RPS3A
RPS7
TPR
UBC
fold change
0.8
0.7
0.6
0.5

Fig. S7. Gene membership in top 10 GO:BP pathways among viral processes genes from Figs. 5 and S4.

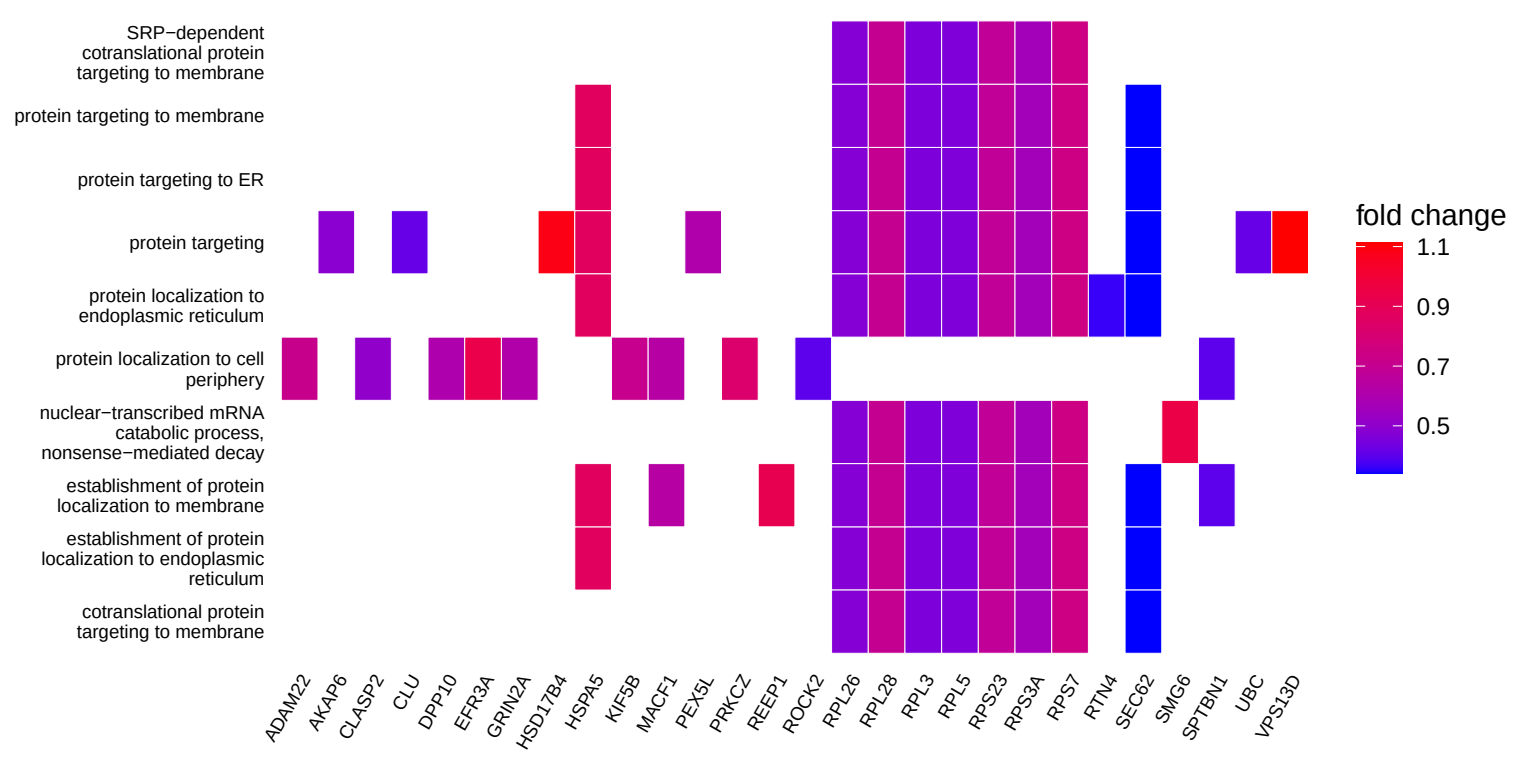
SRP−dependent cotranslational protein targeting to membrane
protein targeting to membrane
protein targeting to ER
protein targeting
protein localization to endoplasmic reticulum
protein localization to cell periphery
nuclear−transcribed mRNA catabolic process, nonsense−mediated decay
establishment of protein localization to membrane
establishment of protein localization to endoplasmic reticulum
cotranslational protein targeting to membrane
ADAM22
AKAP6
CLASP2
CLU
DPP10
EFR3A
GRIN2A
HSD17B4
HSPA5
KIF5B
MACF1
PEX5L
PRKCZ
REEP1
ROCK2
RPL26
RPL28
RPL3
RPL5
RPS23
RPS3A
RPS7
RTN4
SEC62
SMG6
SPTBN1
UBC
VPS13D
fold change
1.1
0.9
0.7
0.5

Fig. S8. Gene membership in top 10 GO:BP pathways among cellular protein localization genes from Figs. 5 and S4.

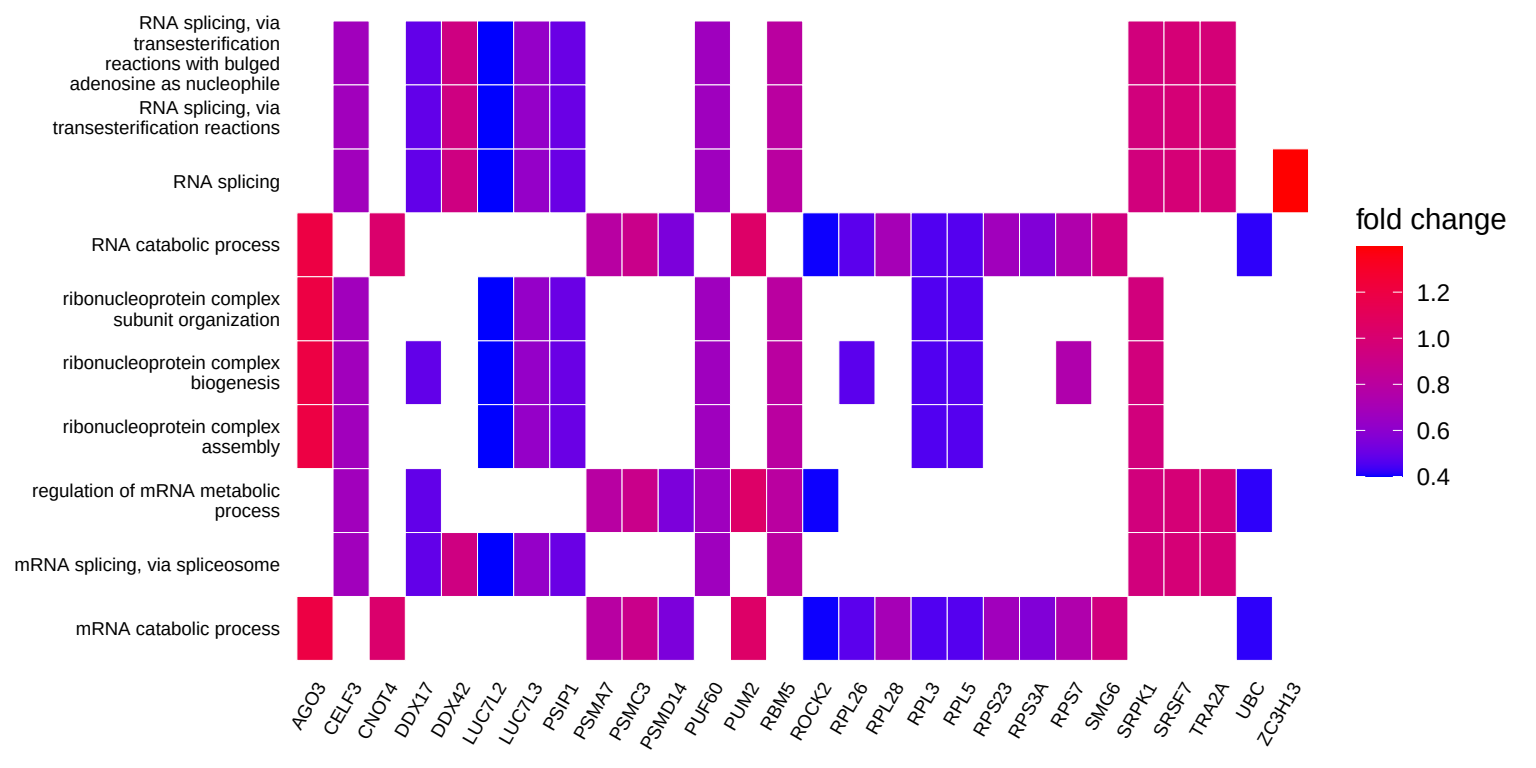
RNA splicing, via transesterification reactions with bulged adenosine as nucleophile
RNA splicing, via transesterification reactions
RNA splicing
RNA catabolic process
ribonucleoprotein complex subunit organization
ribonucleoprotein complex biogenesis
ribonucleoprotein complex assembly
regulation of mRNA metabolic process
mRNA splicing, via spliceosome
mRNA catabolic process
AGO3
CELF3
CNOT4
DDX17
DDX42
LUC7L2
LUC7L3
PSIP1
PSMA7
PSMC3
PSMD14
PUF60
PUM2
RBM5
ROCK2
RPL26
RPL28
RPL3
RPL5
RPS23
RPS3A
RPS7
SMG6
SRPK1
SRSF7
TRA2A
UBC
ZC3H13
fold change
1.2
1.0
0.8
0.6
0.4

Fig. S9. Gene membership in top 10 GO:BP pathways among mRNA metabolic processes genes from Figs. 5 and S4.